#44

QUARTERLY Newsletter

Mercator Ocean
Ocean Forecasters

Credits: SIPA

Credits: REUTERS/HO NEWS.

(Left) On the night of June 1st to June 2nd 2009 at 2h10 GMT, crash of the Air France AF447 flight from Rio to Paris.
(Right) The Fukushima Daiichi nuclear disaster following the Tōhoku earthquake and tsunami on 11 March 2011.

Editorial – January 2012 – Various areas of benefit using the Mercator Ocean products

Greetings all,

Mercator Ocean runs operational services and provides expertise to a large panel of users: scientists, public authorities, agencies and even the private sector. This month's newsletter gives a focus on four areas of benefits. First article is dedicated to the contribution of Météo-France and Mercator Ocean to the research at sea of the wreckage from the Air France AF447 flight from Rio to Paris. Second article presents the contribution of Mercator Ocean and Laboratoire d'Aerologie in order to investigate the dispersion in seawater of radionuclides after the castrophic event of the Fukushima nuclear plant. Third article displays the work done at Mercator Ocean in order to assist Meteo France in predicting the fate of sea pollutions or drifting objects during disasters like oil spills for example. Last article is about the Mercator Ocean state of the art reanalysis product GLORYS2V1 which is of great interest for the climate community.

On the night of June 1st to June 2nd 2009 at 2h10 GMT, the Air France AF447 flight from Rio to Paris disappeared in a highly variable and poorly observed part of the western tropical Atlantic Ocean. The two first phases of research at sea of the AF447 wreckage were both unsuccessful. The "Bureau d'Enquêtes et d'Analyses pour la sécurité de l'aviation civile" (BEA) (for the investigation of airplane accidents) decided in November 2009 to gather a group of ocean scientists and mathematicians in order to prepare the third phase of research. The study performed by Mercator Océan and Météo-France as part of this group is partly described here with a focus on the modelling part of the common contribution of Météo-France and Mercator Ocean as an attempt to improve the currents and winds and consequently the drift accuracy.

After the castrophic event of the Fukushima nuclear plant in March 11 2011, various simulations using the 3D SIROCCO circulation model were performed in order to investigate the dispersion in seawater of radionuclides emitted by the Fukushima nuclear plant. In this framework, Mercator Ocean has provided the initial fields and the lateral open boundary conditions from the global 1/12° system. Moreover, for the MyOcean component of GMES, Mercator Ocean has also calculated the Lagrangian drift of water particles from the global 1/12° ocean system and has set up a weekly web bulletin of the situation of currents published during one year from the date of the disaster.

Predicting the fate of sea pollutions or drifting objects is a crucial need during disasters. In case of incident over the French marine territory, Météo France has the responsibility to provide reliable ocean drift forecasts for authorities and decision makers using the oil spill model MOTHY which is operated on duty 24/7/365. Since 2007, MOTHY is fed with currents forecasted by Mercator Ocean's assimilated systems. Stephane Law Chune et al. presents their work using the Mercator Ocean velocity fields in order to provide better current forecast to Météo France. This cooperation already provided helpful assistance in the past, like during the Prestige incident (10 years ago).

The fourth paper presents the Mercator ocean GLORYS2V1 (1993-2009) global ocean and sea-ice eddy permitting reanalysis over the altimetric era. Main improvements with respect to the previous stream GLORYS1V1 (2002-2009) are shown. Data assimilation diagnostics reveal that the reanalysis is stable all along the time period, with however an improved skill when Argo observation network establishes. GLORYS2V1 captures well climate signals and trends and describes meso-scale variability in a realistic manner.

The next April 2012 issue will be a special publication with a common newsletter between the Mercator Ocean Forecasting Center in Toulouse and the Coriolis Infrastructure in Brest, more focused on observations. We wish you a pleasant reading!

Laurence Crosnier, Editor.

CONTENT

Meteo-France and Mercator Ocean contribution to the search of the AF447 wreckage 3

By M. Drévillon, E. Greiner, D. Paradis, C. Payan, J-M. Lellouche, G. Reffray, E. Durand, S. Law-Chune, S. Cailleau

Mercator Ocean operational global ocean system 1/12° PSY4V1: performances and applications in the context of the nuclear disaster of Fukushima 11

By C. Derval, C. Desportes, M. Drévillon, C. Estournel, C. Régnier, S. Law Chune

Drift forecast with Mercator Ocean velocity fields and addition of external wind/wave contribution 22

By S. Law Chune , Y. Drillet, P. De Mey and P. Daniel

GLORYS2V1 global ocean reanalysis of the altimetric era (1993-2009) at meso scale 28

By N. Ferry, L. Parent, G. Garric, C. Bricaud, C-E. Testut, O. Le Galloudec, J-M. Lellouche, M. Drévillon, E. Greiner, B. Barnier, J-M. Molines, N. Jourdain, S. Guinehut, C. Cabanes, L. Zawadzki.

METEO-FRANCE AND MERCATOR OCEAN CONTRIBUTION TO THE SEARCH OF THE AF447 WRECKAGE

By M. Drévillon[1], E. Greiner[2], D.Paradis[3], C. Payan[3], J-M. Lellouche[1], G. Reffray[1], E. Durand[1], S. Law-Chune[1], S. Cailleau[1]

[1] *Mercator Océan, Ramonville-St-Agne, France*
[2] *CLS, Ramonville-St-Agne, France*
[3] *Météo-France, Toulouse, France*

Introduction

On the night of June 1st to June 2nd 2009 at 2h10 GMT, the Air France AF447 flight from Rio to Paris disappeared in a highly variable and poorly observed part of the western tropical Atlantic Ocean. In the following days the wreckage was not located and the first debris was sighted only 5 days after the accident. From June 10th to July 10th, 2009 (period hereafter called phase 1) several ships including the "Pourquoi Pas?" (Ifremer/SHOM) have conducted acoustic researches to find the beacons. Reverse drift computations were performed by several search-and-rescue groups in the world including at Météo-France, using background ocean currents from Mercator Ocean. The drift computations were started from the debris found from June 5th to June 17th and their backward trajectory until the time of the accident was computed. The results indicated very different locations for the wreckage. All these likely locations were searched during phase 2 (from July 27th to August 17th 2009) using submarine robots. The research conditions were very difficult as the bottom of the ocean is very deep (around 4000m) in that region with a very rugged topography that can be compared to the Alps under 4000m of water. These two phases of research at sea of the AF447 wreckage were both unsuccessful. The "Bureau d'Enquêtes et d'Analyses pour la sécurité de l'aviation civile" (BEA) (for the investigation of airplane accidents) decided in November 2009 to gather a group of ocean scientists and mathematicians in order to prepare the third phase of research. They had to apply new methods to reduce uncertainties in the drift computations and propose a region to begin phase 3. The latter was to start in February 2010 and finally took place from April 2nd to May 24th, 2010. The task of reducing uncertainties was challenging as very little environmental information was available at the time. Moreover the study had to be performed within a short delay (3 months) and only a few more observations were made available during this period. Ollitrault et al. (2010) present in detail the work that was done by the group of scientist hereafter called the "drift committee". The study performed by Mercator Océan and Météo-France as part of this group is described in Drévillon et al. (2012), and includes the operation of an ensemble of numerical experiments to calculate the probability of presence of the wreckage. In this article, we focus on the *modelling part* of the common contribution of Météo-France and Mercator Ocean as an attempt to improve the currents and winds and consequently the drift accuracy.

The common Mercator Océan and Météo-France strategy is outlined in section 2. The numerical experiments that were performed for this study are introduced in section 3. In section 4 we analyse the improvements obtained. A conclusion is drawn in section 5.

Modelling strategy

Scott et al. (2012) pointed out that the performance of any of the available operational ocean current analyses in the region and season of interest was leading to positioning errors ranging from 80 to 100 km after five days of inverse drift computation. This level of accuracy could not allow discriminating a sub-zone within the circle of radius 74 km (40 nm) which was defined by BEA as the maximum area of research around the last known position (LKP) of the airplane at 2°58.8'N and 30°35.4'W. These positioning errors only due to currents mainly come from the ocean model intrinsic errors and errors in the atmospheric forcing fields (including winds) or boundary conditions (bathymetry). The lack of good quality observations also lead to poorly constrained ocean analyses (initial condition errors) as well as for atmosphere analyses.

The highest spatial resolution (1/12° horizontal resolution) analyses of the PSY2V3R1 system for the North Atlantic Ocean and Mediterranean Sea from Mercator Ocean (hereafter referred to as PSY2) are known to be reliable in the Atlantic Ocean (Hurlburt et al. 2009) and were chosen to deliver information on the ocean currents at the time of the accident. While the agreement of PSY2 analyses with temperature and salinity measurements is generally satisfactory, they have poor correlation with the drifter velocity observations (of the order of 0.5). They generally underestimate the current variability in our region of interest (up to 20 % underestimation), and the root mean square differences are of the order of 0.2 to 0.3 m/s (which means locally up to 100% relative errors). This relative poor agreement can be associated with various causes: the system does not assimilate the surface drifters' velocities, the surface layer is difficult to model and there are not enough real time observations to do this data assimilation properly. One can also note that drifters may overestimate the currents in regions of significant winds due to the undetected loss of their drogues (Grodksy et al. 2011).

Errors in the atmospheric forcing fields result in large uncertainties in the ocean current model estimates. Errors in winds are particularly crucial for this study as wind is also used at the drift computation stage. The immersed object movement is subject to both ocean currents and winds, in proportions depending on its rate of immersion. In the atmosphere the non-linearity generates discrepancies with the observations with a smaller time scale than in the ocean. A large amount and homogeneous cover of observations is required in order to properly constrain the analyses that are performed at a high temporal frequency (every 6h in the case of ARPEGE). Rain contaminates satellite scatterometer measurements that allow constraining low level wind in the atmosphere. Thus in periods of strong convective events as during the AF447 accident, the wind analyses have intrinsically a lower quality.

For the phase 3 of research of the AF447 wreckage, the drift committee had to try to produce current and wind estimates with a better accuracy, using modelling and data assimilation techniques, and as much as possible observational data in order to better constrain and/or validate those currents. The time and region of the accident were poorly observed, with only a few in situ measurements and satellite observations that were not representative of the rapidly changing situation (but rather of a weekly average). Thanks to fishermen's solidarity, new surface current measurements were collected by Collecte Localisation Satellite (CLS) during the preparation of phase 3, and were particularly important to achieve this task.

The first concern was to optimise as much as possible the atmospheric and ocean analyses. The atmosphere and ocean operational analysis and forecasting systems could not be modified in such a short delay. Nevertheless, experimental versions of the state-of-the-art systems were developed for this purpose and were used to perform reanalyses for the period surrounding the accident (May and June 2009). This work was performed in autumn 2009 when we were able to assimilate observations that were not yet available or properly controlled in June 2009. The reanalyses were performed separately with ARPEGE for the atmosphere (Météo-France) and PSY2 for the ocean (Mercator Océan) with a particular emphasis on the improvement of the ocean-atmosphere boundary (surface winds and currents).

Then, those reanalyses were used as boundary and initial conditions for several experiments with a small and flexible ocean model limited to the region of interest. This small 12°x10° configuration of NEMO could benefit from recent improvements of the ocean physics representation (mixed layer scheme for instance). Some physical processes were added that are not yet taken into account in the global configuration such as tides and a high frequency atmospheric forcing (3-hour to 1-hour for winds). Due to a relatively low computational cost, several experiments could be performed and validated, and results could be obtained within a short delay. Moreover it was possible to vary the date of the initial conditions (all coming from the optimised ocean analyses) and the type of atmospheric forcings. This small ensemble allowed us to derive information on the sensitivity to these changes of initial conditions and forcings. The best solution was then selected by means of a comparison of drift computations with MOTHY using all available surface drift observations. Various combinations between sets of modelled currents and winds, and between the modelled currents and the drift observations were evaluated. Drifts were also computed with the SURCOUF (CLS) ocean currents deduced with a statistical method (no ocean model) from SLAs (geostrophic component) and winds (Ekman component).

Numerical experiments

The ARPEGE reanalysis: atmospheric conditions

ARPEGE is the operational global weather forecasting system of Météo-France (Auger et al. 2010). It is a stretched model, on a spectral grid and with a semi-implicit semi-Lagrangian temporal scheme. It uses a 4D-VAR algorithm for its data assimilation, every 6 hours. An updated version, that became operational in April 2010, was used as a basis for an atmospheric reanalysis on the May-June 2009 period, with higher resolution (70 vertical levels, 1/5° horizontally on the zone of interest) and changes in the physics (stratiform rain, turbulent scheme). The system was also tuned to improve the atmospheric analysis, by a better specification of observations errors, background errors specified according to the covariance errors of a variational assimilation ensemble (Berre et al. 2007), increasing the number of assimilated satellite radiances, and updating the fast radiative transfer model from RTTOV8 to RTTOV9 (Saunders et al. 2010). For the purpose of this reanalysis, the weight of scatterrometer surface neutral wind observations (Seawinds on QuikScat, AMI on ERS-2, ASCAT on MetOp-2, (Payan 2010)) was multiplied by 4 in the assimilation. For data from Seawinds scatterometer, sensitive to the rain, a change of quality control flag allowed for more data to be assimilated near the rainy patterns (Portabella and Stoffolen 2001; Payan 2008). Finally, hourly outputs were produced in order to provide high temporal resolution information, and higher resolution surface forcings to be applied to ocean models for sensitivity tests.

The PSY2 numerical experiments: ocean currents

The PSY2 configuration including the Mediterranean Sea, Tropical and North Atlantic in its real time operational version (hereafter referred to as PSY2-OPER) uses the version 1.09 of NEMO (Madec, 2008). Its horizontal resolution is 1/12°x1/12° and 50 levels on the vertical, with a refinement of the vertical grid between 0 and 100m (22 levels). The main model parameterizations are listed in Table 1. The SAM2 Data As-

similation software (Tranchant et al. 2008; Cummings et al. 2009) is developed at Mercator Océan and is based on the Singular Evolutive Extended Kalman Filter (SEEK) formulation of Pham et al (1998). In PSY2-OPER along track altimeter Sea Level Anomalies (SLA) from AVISO, the RTG-SST Sea-Surface-Temperature (SST) from NCEP (Thiébaux et al., 2003) together with the temperature and salinity in situ profiles from CORIOLIS (Ifremer) are assimilated together in a fully multivariate way.

The reanalysis (hereafter referred to as PSY2-REANA) differs from the operational version PSY2-OPER mainly by the type of observations that were assimilated. SLAs were post processed (large scale bias corrections, orbit corrections etc…) and temperature and salinity profiles were quality controlled respectively by AVISO and CORIOLIS. The assimilation time window was shortened to 5 days in the PSY2-REANA experiment instead of 7 days in the real time PSY2-OPER system. This allowed putting more weight on the observations at the analysis stage, especially the SST observations.

A zoom *with no data assimilation* was then nested into the PSY2-REANA solution with data assimilation. Rather than performing a grid refinement (the resolution and bathymetry are the same as in PSY2-REANA, at 1/12°), we chose to improve the physics of the model to allow a better representation of small scale processes. The zoom domain chosen is 36°W-24°W and 1°S-9°N. The bathymetry and the grid coordinates come from PSY2-OPER and were directly extracted from its configuration files. The model is initialised with a PSY2-REANA restart file and the lateral boundaries are forced by the outputs of PSY2-REANA with a daily frequency. The sequential data assimilation scheme induces jumps of the solution after the initialisation stage. Thus PSY2-REANA outputs have been filtered (low pass) to ensure the continuity on the boundary forcing and to avoid the generation of spurious waves in the nested zoom domain. The variables considered are: T, S, U, V and SSH. The model features used for the zoom experiments (called PSY2-ZOOM) are compared with those of PSY2-OPER and PSY2-REANA in table 1.

	PSY2-REANA (and -OPER)	PSY2-ZOOM
Vertical coordinate system	z + partial-step + fixed volumes (linear free surface)	z + partial-step + variable volumes (non linear free surface)
Tide	None	7 components (TPXO)
Atmospheric forcings	ECMWF daily for all fields	ECMWF daily for all fields except for the wind stress (3h) for ZOOM2 only: ARPEGE reanalysis wind forcing (1h) are used
Surface boundary condition	CLIO with a constant value for the atmospheric pressure	CLIO including atmospheric pressure effect
ECMWF fields corrections	None	Precipitation corrected by GPCP Cloud cover corrected by ISCCP
Free surface resolution	Filtered with elliptic solver	Time-splitting with tidal and atmospheric pressure effects
Turbulence	TKE	TKE2 (update)
Advection scheme for tracers	TVD (Zalesak, 1979) scheme	QUICKEST+ULTIMATE (Leonard, 1979; 1991)
Lateral tracer diffusion	Laplacian along the isopycnal slopes (125. m2s-1)	None (implicit diffusion in the advection scheme)
Advection scheme for momentum	Vector form : energy and enstrophy conserving scheme	Vector form : energy and enstrophy conserving scheme
Lateral viscosity	Bilaplacian operator along the geopential (-1.25e10 m2s-1)	Bilaplacian operator along the geopential (-1.25e10 m2s-1)
Bottom friction	Non linear (1.e-3)	Non linear (1.e-3)
Density	UNESCO (Jackett and McDougall, 1995)	UNESCO (Jackett and McDougall, 1995)
Solar penetration	Water type I	Water type I

Table 1 : Summary of the model parameterizations that were used in the PSY2 runs and of the main differences between the experiments performed

As detailed in Table 1, PSY2-ZOOM includes the modelling of tides as well as a different parameterization of vertical mixing. The update frequency of the atmospheric forcing is daily (daily averages) for the PSY2-OPER and PSY2-REANA systems, and 3-hourly in the PSY2-ZOOM experiments. In addition, the effect of the atmospheric pressure is taken into account in the bulk formulae of the forcing fields of the embedded PSY2-ZOOM. Two different types of zoom experiments have been performed varying only the origin and frequency of the *wind stress* forcing. In the PSY2-ZOOM1 category 3-hour wind stresses from ECMWF were used, and in the PSY2-ZOOM2 category (only one experiment) 1-hour wind stresses were used, taken from the ARPEGE reanalysis specially tuned for this study. Finally five different experiments were available to

assess the impact of initial condition errors and the impact of atmospheric forcing field errors: in the case of PSY2-ZOOM1 four numerical experiments were started from different dates in order to vary the model initial condition; and a comparison between PSY2-ZOOM2 and PSY2-ZOOM1 experiments gives an estimate of the sensitivity to surface wind errors. All the PSY2-ZOOM experiments have daily averaged 3D output files and instantaneous hourly surface outputs.

The MOTHY drift computations

The drift model MOTHY (Daniel et al., 2002) relies heavily in wind-parameterisation of the currents. The water velocity is provided by a coupling between a 2D hydrodynamic limited area ocean model and a 1D eddy viscosity model. MOTHY only uses external ocean model data from a single depth – typically at the base of the Ekman layer – in the place of a climatological background current, and calculates the main drift component from the wind and tide data. It parameterizes the upper ocean drift from wind speed using a sophisticated Ekman type scheme (Poon and Madsen, 1991). On continental shelves, the 2D model provides a strong constraint to the 1D model by the interaction of currents due to tide, wind and topography. In contrast, above the ocean basins, the combination of currents from operational oceanography systems and wind (1D) leads the drift. This is the case in the region of interest of the western Equatorial Atlantic. Once the currents have been computed, they can be used to evaluate the drift of a body or an object at sea. MOTHY proposes two ways for that: a container model and a leeway model.

In the first case, the main forces on any floating object container type are computed, depending on its immersion rate, and its trajectory is deduced.

In the second case, a Monte Carlo-based stochastic ensemble trajectory model calculates the motion of objects on the sea surface under the influence of wind and surface currents. The output is then an approximation of the time evolving probability distribution (search area) in the form of an ensemble of particle positions. Drifting objects are divided into classes, e.g., a person in water (PIW), various classes of life rafts, small motor boats, etc (Allen and Plourde, 1999; Breivik and Allen, 2008).

In this study the current analyses are thus used in two ways by MOTHY: either the surface currents are prescribed (and MOTHY just adds the wind drag on the emerged part of the objects) or the currents just below the Ekman layer (at an around 30 m depth) were prescribed and the complete Mothy computation was performed. For the PSY2-ZOOM experiments, the outputs were available daily or every hour, thus the impact of the ocean current input frequency could be tested.

With all this variety of input data, the MOTHY system was run in more than 20 different configurations (2 atmospheric models, 5 types of ocean current analyses or models and 2 different current depths). The high frequency oceanic outputs (hourly instead of daily) added 4 more possibilities for the PSY2-ZOOM experiments.

PSY2-ZOOM results

As already mentioned very few in situ drift observations were available and the most representative observations came from floating objects used by fishermen and located every 6h with the ARGOS system. These floats had been used previously by CLS to deduce ocean currents velocities and it was shown that on average they compare well with velocities deduced from Surface Velocity Program SVP drifters (E. Greiner, personal communication). The trajectories of the two most representative buoys were reproduced with MOTHY using all possible couples of input ocean currents and winds. The realism of a trajectory can be measured for instance by the distance between the modelled and the observed ending point. One can also compute the cumulative distance with the observation all along the trajectory. As we focus here only on two buoys the synoptic view of all trajectories is displayed rather than the cumulative scores. Figure 1 shows that the drift computations based on PSY2-OPER send the buoy #42 far north east of its real position. The distance travelled by the buoy is overestimated. The real trajectory sends the buoy approximately half a degree north of its initial position. PSY2-REANA and PSY2-ZOOM currents significantly improve the trajectories with both 90% and 100% immersion rate. SURCOUF also produces a realistic trajectory but seems to underestimate slightly the velocity. The 100% immersion as well as the use of ECMWF winds (referred to as CEP in the figure) also seem to give better results. The second buoy (#246, Figure 2) travels very near the last known position of the plane in space and time. It indicates a constant east-north-eastward displacement that is well reproduced by SURCOUF and PSY2-ZOOM2. PSY2-OPER and PSY2-REANA send the buoy far too much north of its actual final position. The two buoys seem to sample two different regimes, and PSY2-ZOOM2 obtains the best results Other comparisons with drift observations confirm that PSY2-ZOOM2 reduces the error with respect to PSY2-OPER, as well as with respect to PSY2-REANA and SURCOUF with variability in the ranking of the three ocean currents depending on the reference in situ observation and its location in space and time (not shown).

Finally reverse drift computations were computed starting from the first floating debris of the plane sighted by the ship URSULLA on June 5th. The reverse MOTHY drift trajectories obtained using PSY2-REANA and PSY2-ZOOM2 currents, and using either ECMWF or ARPEGE reanalysis winds are displayed in Figure 3. Three different immersions were tested to take into account the uncertainty on the immersion rate. The

dispersion of the results illustrate that it was likely that the wreck was located somewhere in the northern part of the circle, even in the north west, but it was difficult to conclude on a specific area. The other results from the drift committee were consistent with this conclusion.

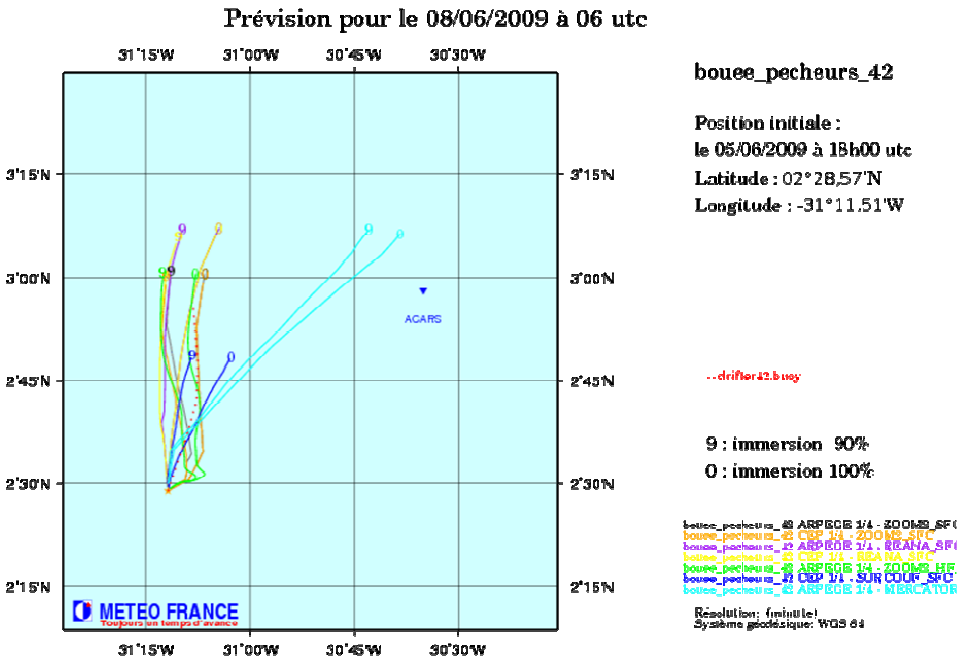

Figure 1 : Synoptic view of several MOTHY forward drift experiments validated with the observed trajectory of a fishermen buoy (#42, red dots). The initial position of all trajectories is indicated on the right, with a color legend for the input current and wind used for each drift. Two different immersions are tested: 90% and 100%. The ACARS point indicates the last know position of the plane.

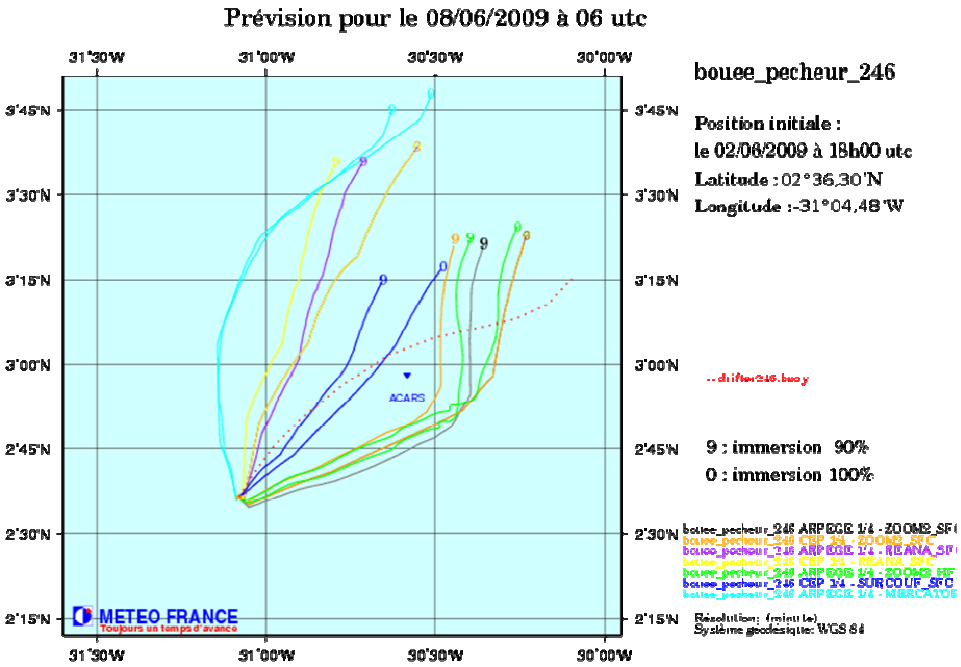

Figure 2 : Same as Figure 1 but for the fishermen buoy #246

Conclusion

In the context of a large international effort to find the wreckage of the AF447 flight after its disappearance in very difficult weather and oceanic conditions in the Tropical Atlantic, Météo-France and Mercator Ocean tried to improve as much as possible their ocean current and wind estimates as well as Météo-France drift model MOTHY. This experience gave rise to fruitful exchanges with the scientists of the "drift committee", and a strengthening of the partnership between the two operational operators Météo-France and Mercator Océan. Tailored reanalyses were performed and local refinement of the model was used to produce an ensemble of "zoom" experiments. It was demonstrated that the tailored experiments reduced the errors with respect to observed drifts. The PSY2-ZOOM2 experiment forced with ARPEGE gave the best performance in all respects. These results were confirmed with several methods (cf Ollitrault et al, 2010) and this PSY2-ZOOM2+MOTHY backward trajectories were finally used for the definition of the search zone, together with estimations from other models run by the drift committee members.

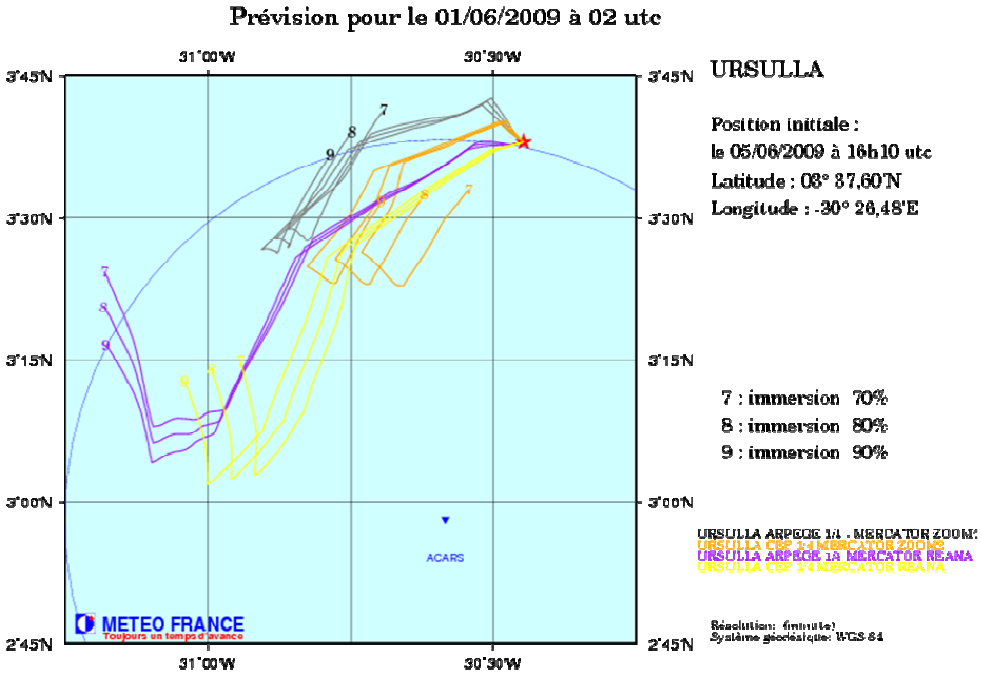

Figure 3 : Synoptic view of several MOTHY backward drift experiments starting from the position of the first debris of the plane sighted by the ship Ursulla on June 5th, 2009.

However, the lack of independent and reliable drift observations uniformly distributed in space and time for the period and for the region of the accident prevented us from making a definitive conclusion on the reduction of uncertainties. The convective cells at the time of the accident resulted in many satellite wind measurements flagged as bad. Thus uncertainty on the winds at the time of the accident remains significant.

This experience confirms that in case of accident at sea, it is necessary to launch drifting floats as much as possible on a large scale zone and as soon as possible after the accident.

This work also stresses the need for assimilation of reliable velocity observations in the operational oceanography systems. The Mercator Océan systems should benefit from this update in the coming years. The challenging work of the drift committee and the very tough work for the teams at sea during phase 3 finally lead to no discovery. Hopefully the wreckage was finally located during a fourth phase of research at sea in 2011. The location of the wreckage was found a few miles North West of the LKP, near 3°02'N and 30°33'W. This location did not fall in the small consensus zone indicated by the drift committee, but was not inconsistent with the ensemble of results that were obtained. The deterministic approach and the selection of one model against all other models are not trustworthy in such an under-observed situation. Ensemble and probabilistic approaches, using a variety of current and wind estimates and crossing different analysis viewpoints do bring useful information.

Acknowledgements

This work was partly supported by BEA. Many thanks to Pierre Daniel (Météo-France), Eric Dombrowsky (Mercator Océan), Yann Drillet (Mercator Océan), Stéphanie Guinehut (CLS), Julien Negre (Météo-France), Dominique Obaton (Mercator Océan), Charly Régnier (Mercator Océan), Marie-Hélène Rio (CLS), Marc Tressol (Mercator Océan) for their contribution to this work. The authors also thank the members of the drift committee Michel Ollitrault (IFREMER), Bruno Blanke (CNRS), Changsheng Chen (UMass), Nicolai Diansky (INM RAS), Fabien Lefevre (CLS), Richard Limeburner (WHOI), Pascal Lezaud (IMT) , Stéphanie Louazel (SHOM), George Nurser (NOC), Robert Scott (NOC) and Sébastien Travadel (BEA) for this challenging team work and many fruitful interactions. Thanks to the reviewers of the drift committee report Laurent Bertino (NERSC), Fraser Davidson (DFO), Valérie Quiniou (Total) and Carl Wunsh for their support and constructive critics. We finally thank the BEA team and especially Johan Condette and Olivier Ferrante for a very interesting cooperation, and congratulate the researchers at sea for this impressive work.

References

Allen A. and J. Plourde, 1999: Review of Leeway: Field Experiments and Implementation, *Technical Report CG-D-08-99*, US Coast Guard Research and Development Center, USA.

Auger L., Bazile E., Berre L., Brousseau P.,. Bouteloup Y, Bouttier F., Bouyssel F., Descamps L., Desroziers G., Fourrié N., Gérard E., Guidard V., Joly A., Karbou F., Labadie C., Loo C., Masson V., Moll P., Payan C., Piriou J.-M., Rabier F., Raynaud L., Rivière O., Seity Y., Sevault E., Taillefer F., Wattrelot E., Yessad K. (2010): The 2010 upgrades of the Météo-France NWP system. *WMO CAS/JSC WGNE Blue Book*, Edited by J. Côté.

Berre L., Pannekoucke O., Desroziers G., Sxtefa˘nescu S. E., Chapnik B., and Raynaud L., 2007:A variational assimilation ensemble and the spatial filtering of its error covariances: Increase of sample size by local spatial averaging. Proc. *ECMWF Workshop on Flow-Dependent Aspects of Data Assimilation, Reading, United Kingdom, ECMWF*, pp 151–168. [Available online at http://www.ecmwf.int/publications/library/do/references/list/14092007.]

Breivik O., Allen A. (2008) An operational search and rescue model for the Norwegian Sea and the North Sea, *Journal of Marine Systems*, 69(1-2):99-113.

Cummings, J., L. Bertino, P. Brasseur, I. Fukumori, M. Kamachi, M.J. Martin, K. Mogensen, P. Oke, C.E. Testut, J. Verron, and A. Weaver (2009) Ocean Data Assimilation Systems for GODAE. *Oceanography*, 22(3):96-109.

Daniel P., Jan G., Cabioc'h F., Landau Y.and Loiseau E. (2002) Drift modeling of cargo containers, Spill Science & Technology Bulletin, Vol. 7(5-6):279-288

Drévillon M., E. Greiner, D. Paradis, C. Payan, J-M Lellouche, G. Reffray, E. Durand, S. Law-Chune, S. Cailleau (2012, in revision) A strategy for producing refined currents in the Equatorial Atlantic in the context of the search of the AF447 wreckage. *Ocean Dynamics SAR special issue.*

Grodsky S. A., Lumpkin R., Carton J. A. (2011) Spurious trends in global surface drifter currents *Geophysical Research Letters*, 38(L10606) doi:10.1029/2011GL047393

H.E. Hurlburt, G.B. Brassington, Y. Drillet, M. Kamachi, M. Benkiran, R. Bourdallé-Badie, E.P. Chassignet, G.A. Jacobs, O. Le Galloudec, J.-M. Lellouche, E.J. Metzger, P.R. Oke, T.F. Pugh, A. Schiller, O.M. Smedstad, B. Tranchant, H. Tsujino, N. Usui, and A.J. Wallcraft. (2009). High-Resolution Global and Basin-Scale Ocean Analyses and Forecasts, *Oceanography* 22(3): pp110–127, doi:10.5670/oceanog.2009.70.

Jackett, D. R., and T. J. McDougall (1995): Minimal adjustment of hydrographic profiles to achieve static stability. J. Atmos. Oceanic Technol., 12, 381–389.

Leonard B. (1979) Stable and accurate convective modeling procedure based on quadratic upstream interpolation. *Computer Methods In Applied Mechanics and Engineering*, 19(1):59–98.

Madec G. (2008): "NEMO ocean engine". *Note du Pole de modélisation*, Institut Pierre-Simon Laplace (IPSL), France, No 27 ISSN No 1288-1619.[Available online at http://www.nemo-ocean.eu/content/download/15482/73217/file/NEMO_book_v3_3.pdf]

Ollitrault M., Blanke B.,Chen C, Diansky N., Drévillon M.,Greiner E., Lefevre F., Limeburner R., Lezaud P., Louazel S., Nurser G., Paradis D., Scott R. (2010) Estimating the wreckage location of the Rio-Paris AF447, *BEA report*, [Available online at http://www.bea.aero/en/enquetes/flight.af.447/phase3.search.zone.determination.working.group.report.pdf]

Payan C. (2008) Status on the Use of Scatterometer Data at Meteo France. *International Winds Workshop Proceedings (IWW9)*. Annapolis (MD - USA) 14-18 April 2008

Payan C.(2010) Improvements in the Use of Scatterometer Winds in the Operational NWP System at Meteo France. *International Winds Workshop Proceedings (IWW10)*. Tokyo (Japan) 22-26 February 2010

Pham D. T., Verron J. , Roubaud M. C. (1998) A singular evolutive extended Kalman filter for data assimilation in oceanography. *Journal of Marine Systems*, 16(3-4):323–340.

Poon Y. K. and O. S. Madsen, 1991: A two layers wind-driven coastal circulation model. *Journal of Geophysical Research*, 96(C2):2535-2548.

Portabella M., Stoffelen, A. (2001) Rain Detection and Quality Control of SeaWinds. *J. Atm. and Oceanic Tech.*, 18:1171-1183

Thiébaux J., E Rogers, W Wang, and B Katz, 'A new high resolution blended real time global sea surface temperature analysis', *Bulletin of the American Meteorological Society, 84,* 645-656, (2003).

Tranchant B., Testut C.E., Renault L., Ferry N., Birol F. and Brasseur P.(2008) Expected impact of the future SMOS and Aquarius Ocean surface salinity missions in the Mercator Ocean operational systems: New perspectives to monitor ocean circulation, *Remote Sensing of Environment*, 112:1476-1487.

Saunders R.W., Matricardi M., Geer A., Bayer P., Embury O.and Merchant C. (2010) RTTOV-9 Science and Validation Report. NWPSAF-MO-TV-020, 74 pp.

Scott R. B., C. N. Barron, M. Drévillon, N. Ferry, N. C. Jourdain, J.-M. Lellouche, E. J. Metzger, M.-H. Rio, O. M. Smedstad (2012, in revision) Estimates of surface drifter trajectories in the Equatorial Atlantic: a multi-model ensemble approach. *Ocean Dynamics SAR special issue.*

Zalesak (1979) Fully multidimensional flux-corrected transport algorithms for fluids. *Journal of Computational Physics*, 31(3):335–362.

MERCATOR OCEAN OPERATIONAL GLOBAL OCEAN SYSTEM 1/12° PSY4V1: PERFORMANCES AND APPLICATIONS IN THE CONTEXT OF THE NUCLEAR DISASTER OF FUKUSHIMA

By C. Derval[1], C. Desportes[1], M. Drévillon[1], C. Estournel[2], C. Régnier[1], S. Law Chune[1]

[1]Mercator Océan, 8-10 rue Hermes, Parc technologique du canal, 31520 Ramonville St Agne
[2]Laboratoire d'Aérologie, 14 avenue Edouard Belin 31400 Toulouse

Introduction

The current Japanese complex crisis is encompassing several natural and industrial disasters, i.e. seism, tsunami and nuclear accident. If the critical impact for the Japanese population is indeed overland, the Japanese authorities announced the extension of the pollution to the marine environment near the Fukushima nuclear power plant with measured levels of radioactive iodine representing 1,250 times the legal limit at sea.

The SIROCCO team (Laboratory of aerology, OMP, Toulouse) has performed, at the request of the International Atomic Energy Agency (IAEA), simulations using the 3D SIROCCO circulation model to investigate the dispersion in seawater of radionuclides emitted by the Fukushima nuclear plant. In this framework, Mercator Ocean has provided since 2011 March 17 the initial fields (T, S, U, V, SSH) and the lateral open boundary conditions from the global system PSY4: one field per day, horizontal resolution 1/12° x 1/12°.

Moreover, for the MyOcean component of GMES, Mercator Ocean has calculated the lagrangian drift of water particles from the analysis provided by the global ocean system PSY4 since March 12th, 2011. Mercator Ocean has also set up a weekly bulletin of the situation of currents from the PSY4 system in this area published for one year from the date of the disaster.

In a first part, the general circulation in the North Pacific is detailed. In a second part, the global system PSY4 is described, and its performance in the area of interest is presented. The last part contains the applications carried out following the Fukushima nuclear disaster.

Description of ocean circulation in the North Pacific

The Pacific North Equatorial Current bifurcates usually between 12°N and 13°N near the east coast of the Philippines (Figure 1). Its branch flowing northward is the Kuroshio Current and the branch flowing southward is the Mindanao current. The Kuroshio Current is a warm current (like the Gulf Stream in the North Atlantic) that carries tropical waters with a temperature up to 25°C towards the polar region. Its trajectory meets the Luzon Strait, flows northward off the east coast of Taiwan then enters the East China Sea. Around 128°E-129°E and 30°N, the Kuroshio Current separates from the continental slope and veers to the east toward Japan islands through the Tokara Strait. Upstream part of the water carried by the Kuroshio Current feeds the Tsushima current flowing northward along the coast of western Japan. The mixing of the cold continental waters and the Kuroshio warm waters gives birth to the Tsushima Current. The Kuroshio Current continues its path towards northeast, along the Ryukyu islands and the Japanese coast and leaves the coast around 35°N and 140°E: this branch of the current is called the Kuroshio Extension, flowing eastward. There are two quasi-stationary meanders east of Japan, with peaks located at 144°E and 150°E. These meanders result from the topography of the Izu Ridge (Figure 2).

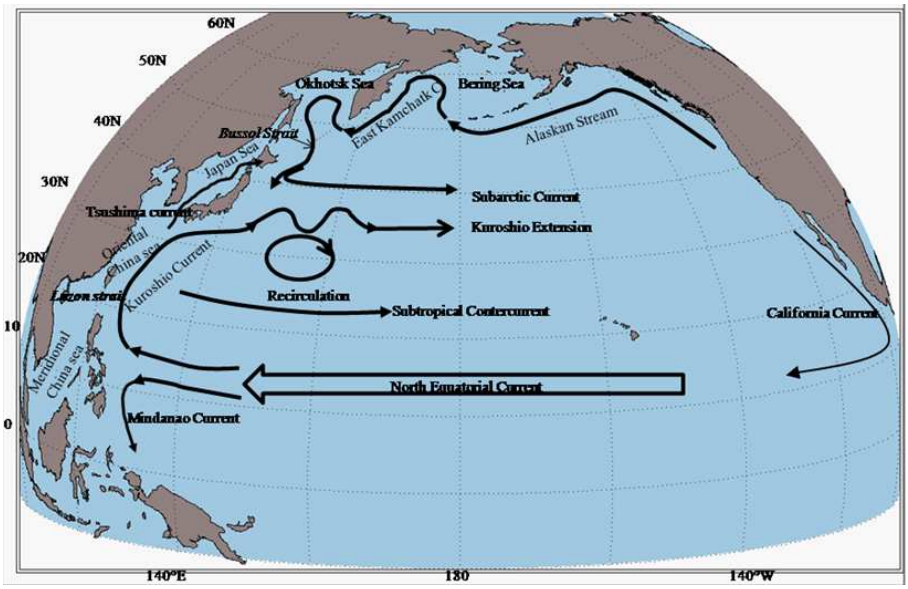

Figure 1 : Schematic description of the North Pacific Circulation (Mercator Océan, QIU 2001, 2010)

The Shatsky Ridge, located near 159°N, is the point where the Kuroshio Extension bifurcates: its main branch flows eastward and the second branch towards northeast up to 40°N where it meets the subarctic current flowing eastward. After crossing the Seamounts Emperor Mountains around 170°E, the Kuroshio path expands and flows in a multi-jet structure. East of the date line, the distinction between the Kuroshio Extension and the Subarctic Current is not clear and they together form the North Pacific current flowing eastward. The Kuroshio is a hun-

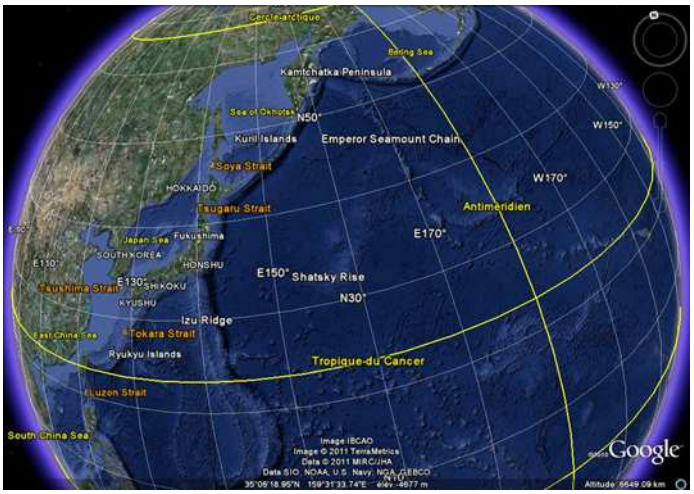

Figure 2 : North Pacific topography

dred kilometres wide and its speed can reach 2 m/s. Compared to the Gulf Stream, its salinity is lower and the influence of cold winds blowing offshore can lead to surface temperature values of about 9° C in some places. The Kuroshio penetrates to a depth of about 1200m to 140°E.

The area of the Kuroshio Current is one of the regions with the highest kinetic energy in the Pacific Ocean.

East of the basin, the Alaskan Current flowing south-westward along the Aleutian Islands, the deep passes between 168°E and 172°E allow its intrusion into the Bering Sea where the Bering Gyre is formed. The branch of this gyre, going to the West becomes the East Kamchatka current flowing to the south west, along the Kuril Islands. Part of the water of this stream penetrates the deep basin of Okhotsk and emerges through the Strait of Bussola where they join the main branch of the Kamchatka current to form the cold Oyashio Current which average temperature is 5°C in winter and between 10 and 15° C in summer.

After following the Hokkaido coast, the Oyashio Current divides into two branches: the first one, around 42°N feeds the Subarctic Current which is characterized by a subarctic front distinct in temperature and salinity of fresh and cold waters from the north and warm and salty subtropical waters. The second one flows southward along the coast of Honshu, and usually reaches 38.7°N and 37°N during specific periods. The southward intrusion of the Oyashio Current, which depends on the years, has a great influence on the hydrographic conditions east of Honshu and on the fishing conditions and regional climate, with a cooling trend in eastern Japan.

The Global Mercator System PSY4

The PSY4V1 (Drillet et al., 2008) ocean model component is built from the OGCM NEMO 1.09 [Madec, 2008]. It consists of an eddy resolving global ocean model coupled to the sea ice model LIM2 [Fichefet and Gaspar, 1988]. The grid is a global quasi isotropic ORCA-type grid with a resolution of 1/12° with 4322X3059 points. The vertical resolution based on 50 levels with layer thickness ranging from 1m at the surface to 450 at the bottom. The vertical coordinate is z-level with partial steps [Barnier et al., 2006].

The global bathymetry is processed from ETOPO2V2 bathymetry. The model is forced by daily mean analyses provided by ECMWF using the CLIO bulk formulae [Goosse et al., 2001]. The PSY4V1 assimilation system is based on the SAM2v1 tool which is a multivariate assimilation algorithm derived from the Singular Extended Evolutive Kalman (SEEK) filter analysis method [Pham et al., 1998]. The analysis provides a 3D oceanic correction (TEM, SAL, U, V), which is applied progressively during the model integration by using the IAU method (Incremental Analysis Update). To minimize the computational requirements, the analysis kernel in SAM2V1 is massively parallelized and integrated in the operational platform hosting both the SAM2 kernel families via the PALM software [Piacentini et al., 2003].

The operational system PSY4V1 is operated at Mercator Ocean since August 2010 and provides weekly 7 days – forecasts.

Validation of the global system PSY4V1R3

Currents

Monthly means of PSY4V1R3 surface current velocity and sea surface height for March 2011 are drawn in Figure 3 to illustrate the main topic of this document. The Kuroshio path and the Kuroshio Extension are well visible, as well as the main eddy north-east of Japan. We can also note the Tsushima current and some cyclonic eddies in the recirculation zone south of Kuroshio and Kuroshio Extension paths.

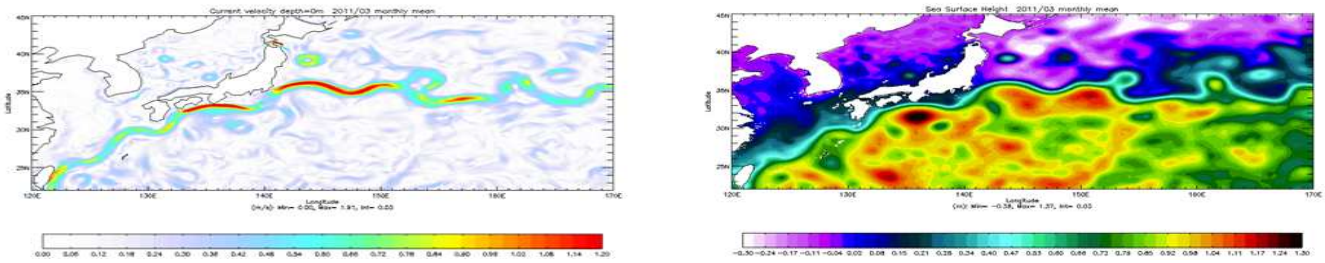

Figure 3 : PSY4V1R3 sea surface current velocity (upper, m/s) and sea surface height (lower, meters), monthly mean, March 2011.

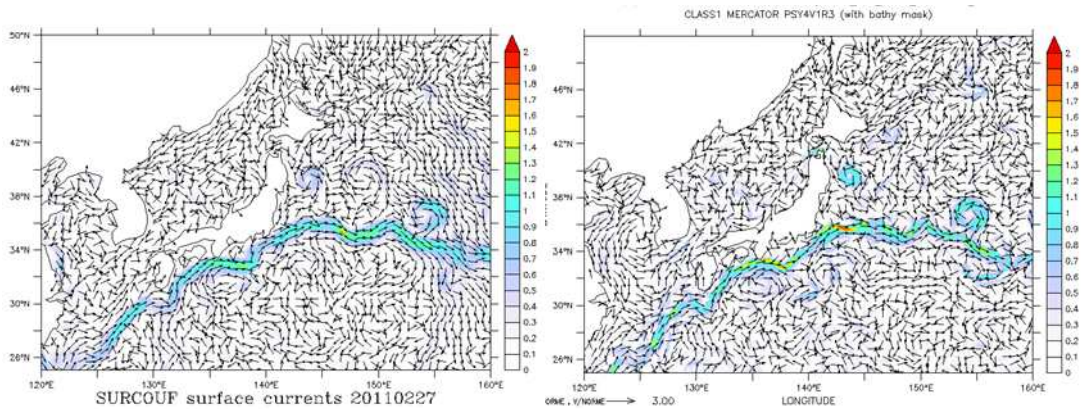

Figure 4 : North Pacific topography Surface currents velocity (m/s) for the 2011, February 27th. Left: SURCOUF, right: PSY4V1R3

The same patterns can be found on surface temperature and salinity (Figure 6 and Figure 7). The Kuroshio path appears clearly to be the boundary between two different zones: the cold and fresh waters coming from the Subarctic Gyre at north, the warm and salty subtropical waters at south.

Surface velocities from a daily analysis are depicted on Figure 4 to illustrate smaller time scale. They are compared with SURCOUF analyses at the same date. The Kuroshio, its extension and the main eddies are well positioned, whereas the velocities seem slightly overestimated. It is worth noting here that SURCOUF, as well as ARMOR3D (Guinehut et al. 2012), use altimetry fields at 1/3° and thus have less energy than PSY4V1R3 daily fields, which represent smaller scales. Due to the limitations of the current observation network and data assimilation systems, the small scales are not constrained. Moreover the errors in general are larger near the coast for all products using altimetry.

The comparison between both surface currents, especially their directions, and the wind velocity at 10m (Figure 5) could let us think that the Ekman component is sometimes underestimated: the blast of wind east of the map does not appear to affect PSY4V1R3 surface current strength and direction. Further investigations are needed to determine if the Ekman model used by SURCOUF (Guinehut et al. 2012), fitted on drifter velocities, does not on the contrary overestimate the Ekman component of the current.

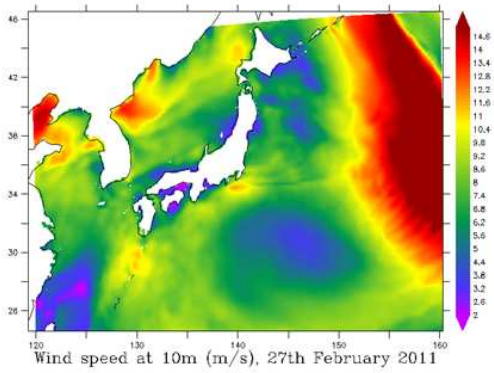

Figure 5 : Wind speed at 10 meters (m/s) for the 2011, February 27th

Temperature and salinity - Comparison with ARMOR-3D

ARMOR3D combines satellite data and *in-situ* observations (synthetic profiles obtained from SLA and objective analysis of all profiles) in order to produce 3D temperature and salinity estimations. Figure 6 and Figure 7 show a comparison between PSY4V1R3 and ARMOR3D analyses at 2 different depths. ARMOR3D is a lot smoother than PSY4V1R3 and is thus unable to reproduce small eddies, fine-scale structures or coastal dynamics, anyway we can see that the main structures are well reproduced.

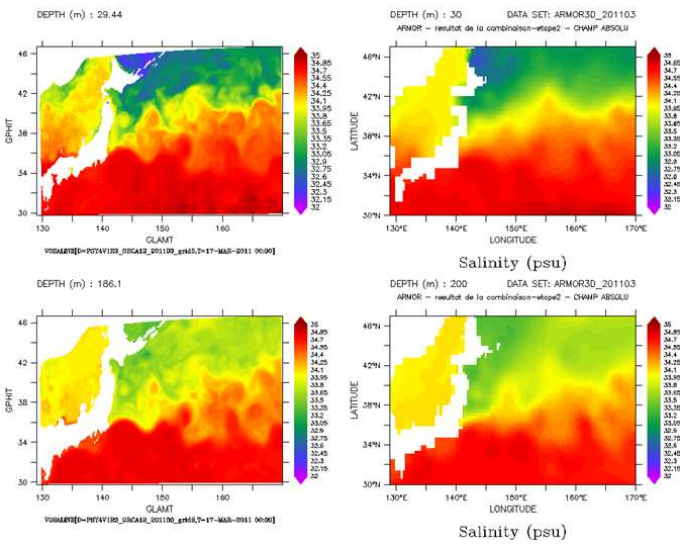

Figure 6 : Salinity (PSU) at 30 meters (upper) and 200 meters depth (lower) for PSY4V1R3 (left) and ARMOR3D analyses, monthly mean, March 2011.

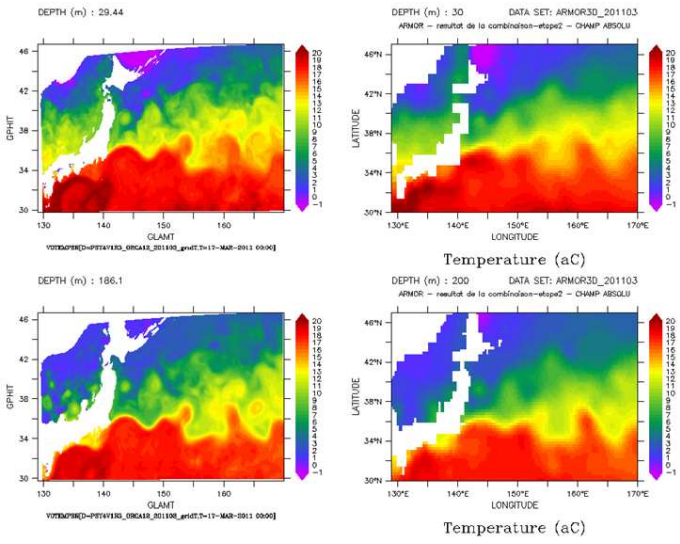

Figure 7 : Temperature (°C) at 30 meters (upper) and 200 meters depth (lower) for PSY4V1R3 (left) and ARMOR3D analyses, monthly mean, March 2011.

Figure 8 focuses on a vertical section at 144°E toward north to further analyse the dynamics near the Kuroshio-Oyashio zone. PSY4V1R3 is compared to ARMOR3D analyses. Temperature and salinity gradients are quite well reproduced by the models. As can be seen also in Figure 6 and Figure 7, the eddy around 39°N is far weaker in ARMOR3D. Mean SURCOUF surface velocity for March 2011 is drawn on Figure 9 and can be compared with the mean current for PSY4V1R3 to see that the intensity of this eddy is slightly overestimated in the model.

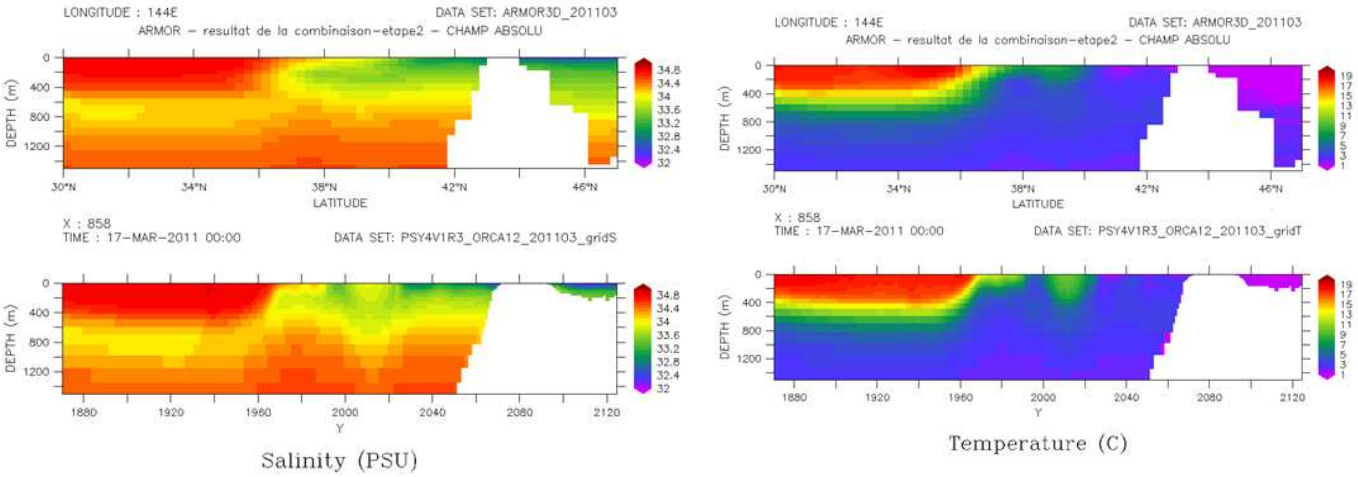

Figure 8 : Salinity (left, PSU) and temperature (right, °C), vertical section along the meridian 144°E of ARMOR3D analyses (upper), PSY4V1R3 (lower), monthly mean, March 2011.

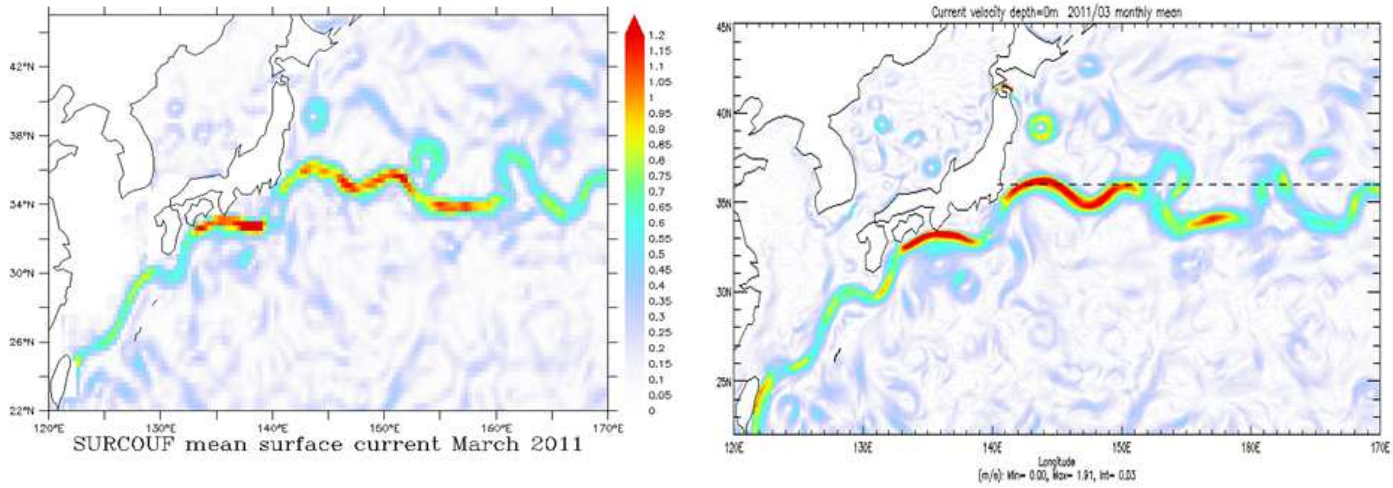

Figure 9 : SURCOUF (left) and PSY4V1R3 (right) sea surface current velocity (m/s), monthly mean, March 2011. The colorbar is the same for both maps. The location of the section used below is added on the map (dashed line).

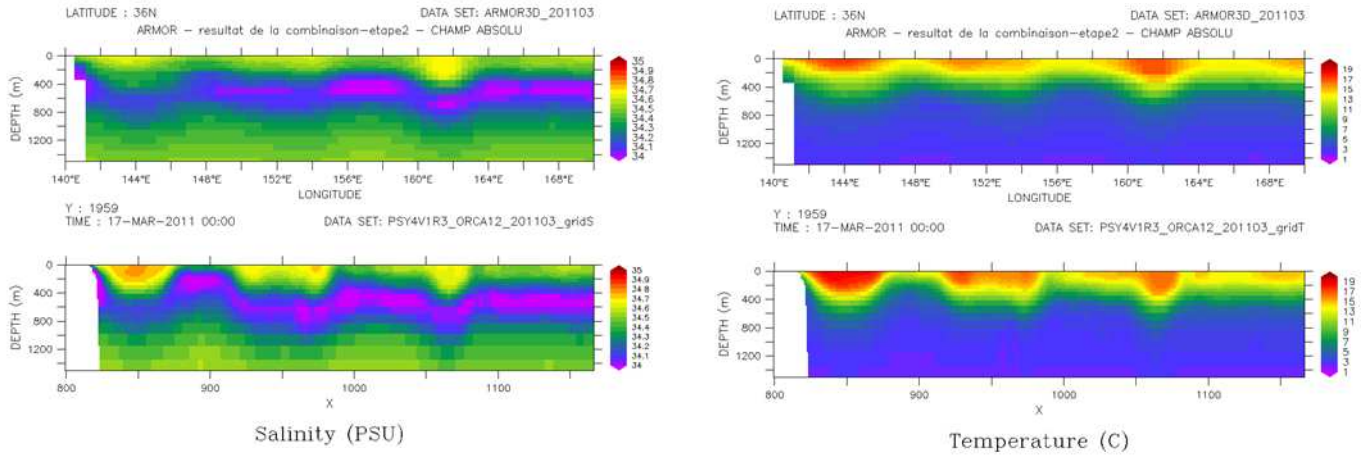

Figure 10 : Salinity (left, PSU) and temperature (right, °C), vertical section along the parallel 36°N of ARMOR3D analyses (upper), PSY4V1R3 (lower), monthly mean, March 2011

The same observations can be done on Figure 10 that is similar to Figure 8 but on a section along the parallel 36°N, that crosses the Kuroshio path in several points (see the dashed line on Figure 9 for location). The western part of the NPIW appears well on the salinity section.

Time series

Mooring

Hourly in-situ temperature and salinity from the Kuroshio Extension Observatory (KEO) site, in the recirculation zone (see position in Figure 11), are plotted in Figure 12 for a nine months period beginning in August 2010. They are compared to the PSY4V1R3 equivalent. Figure 13 shows other variables for PSY4V1R3. At the beginning of the period, a cyclonic eddy, propagating westward, meets the mooring (mooring data are not available at the time). Fresh and cold water is upwelled (positive vertical velocity). Around January, we can note the seasonal change in water masses characteristics, well represented in the model and confirmed by in-situ data: near surface waters become colder and saltier, the vertical diffusivity increases as the mixed layer depth becomes deeper.

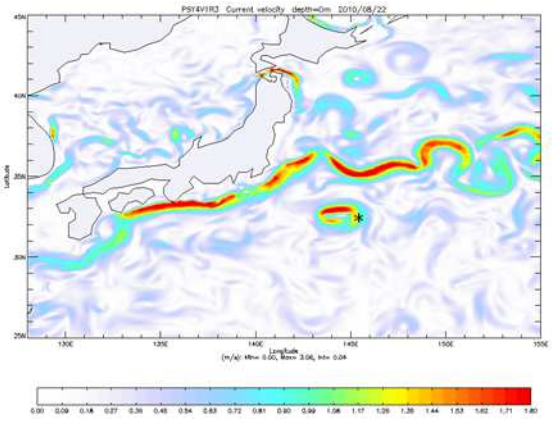

Figure 11 : PSY4V1R3 sea surface current velocity (m/s), 22nd August 2010. The position of the mooring (cross at 145.5E, 32.4N) is added on the map.

Comparison with RTG-SST observations

Surface temperature in this zone is quite well reproduced by PSY4V1R3, as can be seen on Figure 14 that compares daily mean SST in Kuroshio region to observed SST. Note that this region (130°E to 170°E, 30°N to 45°N, see Figure 6: for example) includes the Japan Sea, often fresher (especially during winter) and colder than the eastern coast of Japan.

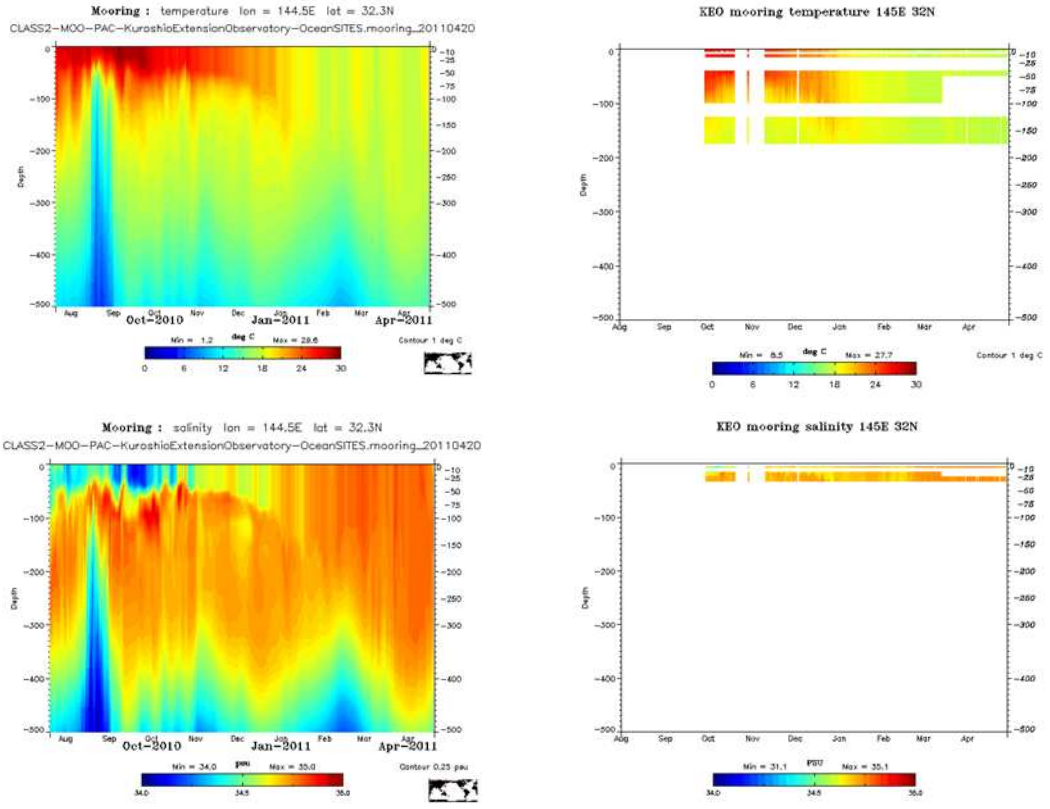

Figure 12 : Mooring at (145.5E, 32.4N): temperature (upper panel, °C) and salinity (lower panel, PSU). Left: synthetic mooring from PSY4V1R3. Right: mooring data from the Kuroshio Extension Observatory (KEO) site.

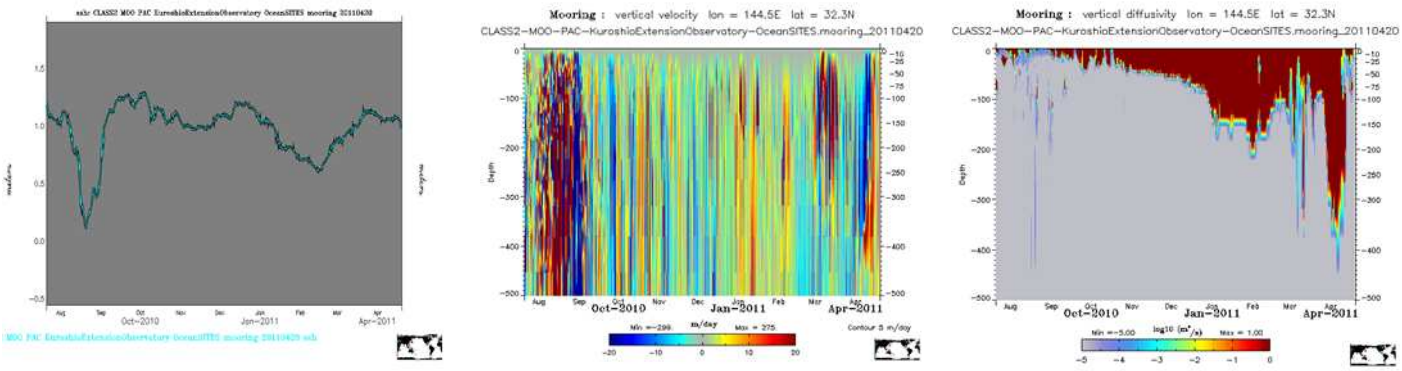

Figure 13 : Synthetic mooring from PSY4V1R3 at (145.5E, 32.4N). Left: sea surface height (m), middle: vertical velocity (m/day), right: vertical diffusivity (log10 (m²/s)).

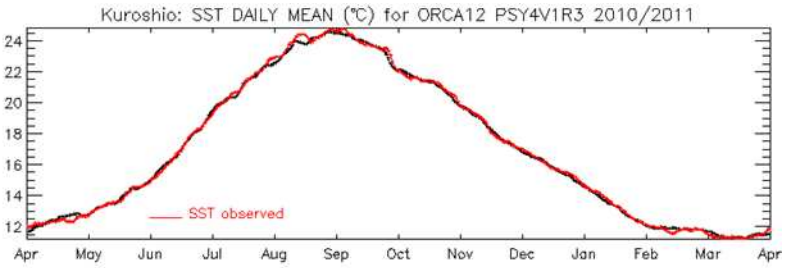

Figure 14 : Daily SST (°C) mean in Kuroshio region, for a one year period ending in April 2011, for PSY4V1R3 (in black) and RTG-SST observations (in red).

Accuracy, comparison with observations

Data assimilation performance

Data assimilation of altimetry and SST reach the expected level of performance in the North Pacific region, as shown in the QuOVaDis (Drevillon et al. 2011) issues. We chose to display here mainly in situ data comparisons as part of the region is close to the coast.

As can be seen on Figure 15, in the North Western extratropical Pacific ocean PSY4V1R3 is too warm (0.3°C) and too salty (0.1 psu) near 100m: negative innovations tend to cool down the model. This bias is seasonal, stronger in summer when the model is stratified (not shown), suggesting mixing problems. Under 500m the biases disappear. PSY4V1R3 does not benefit from seasonal bias correction like the more up-to-date PSY3V3R1 (global 1/4°), nevertheless no bias can be detected at depth in PSY4V1R3.

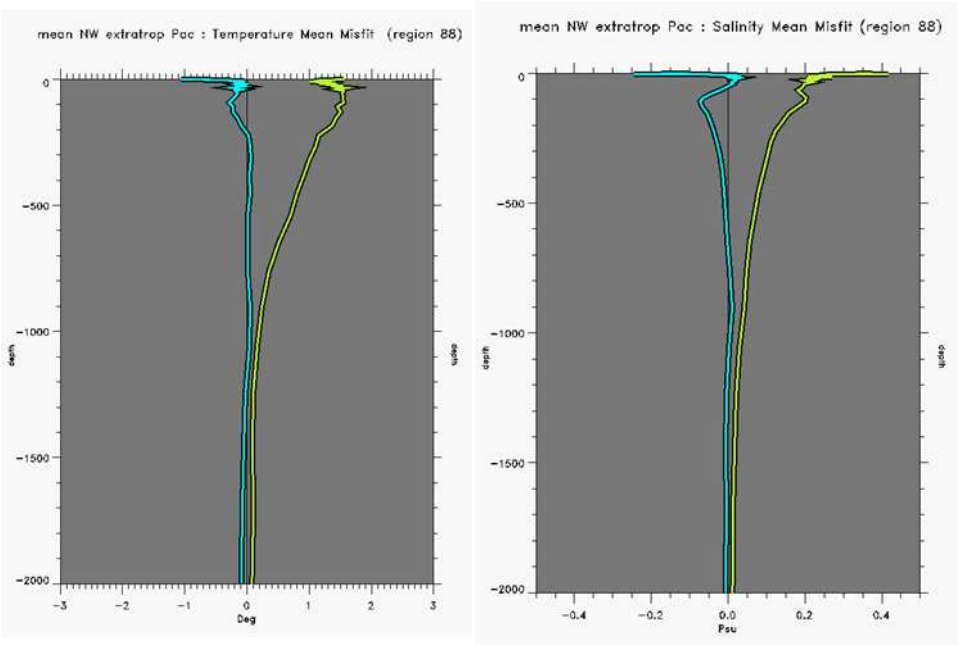

Figure 15 : mean 2010 temperature profiles (left, °C) and salinity profiles (right, PSU) of average of innovation (blue) and RMS of innovation (yellow) on the north western extratropical Pacific Ocean (120 to 190 °E, 30 to 60 °N), for PSY4V1R3.

Daily products compared to observations

The great amount of in-situ observations in this region is noteworthy and allows us to draw reliable plots and to provide rather trustworthy statistics.

Temperature and Salinity profiles

As can be seen in Figure 16, salinity and temperature errors in the 0-500m layer are usually less than 0.2 psu and 1°C. The area of high mesoscale variability displays higher errors that can reach 0.3 to 0.5 psu and 2°C.

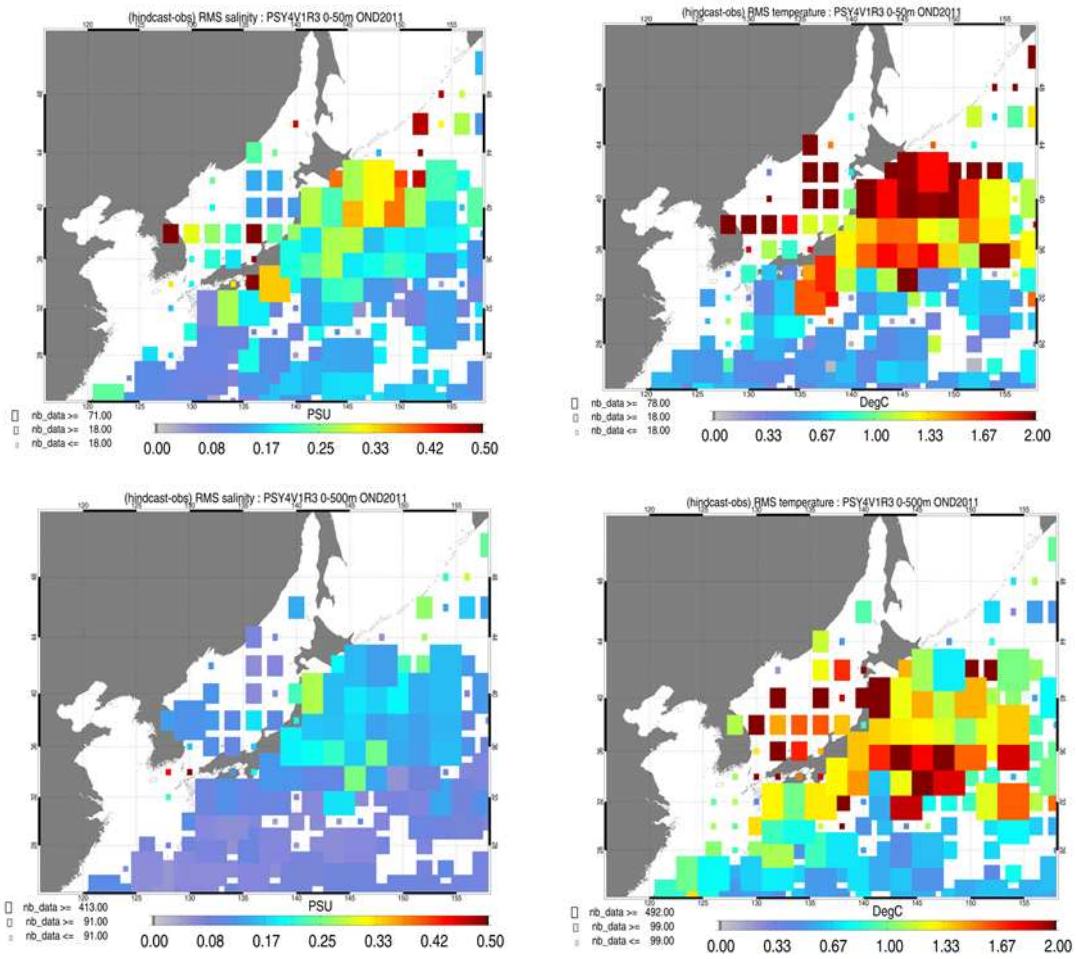

Figure 16 : Spatial distribution of the salinity (left, PSU) and temperature (right, °C) RMS error departures from the observations in the PSY4V1R3 system in October-November-December 2011, averaged in the 0-50 m layer (upper) and in the 0-500m layer (lower). The size of the pixel is proportional to the number of observations used to compute the RMS in 2°x2° boxes.

Water masses diagnostics

Daily PSY4V1R3 analyses are collocated with in-situ profiles of temperature and salinity from Coriolis database, to draw the Theta-S diagrams of Figure 17. Levitus WOA05 is collocated as well with in-situ profiles for comparison. Three water masses with different characteristics appear. The Japan Sea region seems quite homogeneous in salt and temperature at depth. The region displayed in the middle plot shows a great spread of water masses characteristics and may contain a small quantity of warm Kuroshio Current water. South of Kuroshio, waters are clearly warmer and saltier. For all these three regions, the diagrams show a good agreement between model and observations: PSY4V1R3 gives a realistic description of water masses in this region.

Using PSY4 in the context of the nuclear disaster of Fukushima

Dispersion in seawater of radionuclides by the SIROCCO model

The SIROCCO team (Laboratory of aerology, OMP, Toulouse) has performed, at the request of the International Atomic Energy Agency (IAEA), simulations using the 3D SIROCCO ocean circulation model to investigate the dispersion in seawater of radionuclides emitted by the Fukushima nuclear plant. The model uses a stretched horizontal grid with a variable horizontal resolution, from 600m x 600m at the nearest grid point from Fukushima, to 5km x 5km offshore. Mercator Ocean provides since 2011 March 17, the initial fields (T, S, U, V, SSH) and the lateral open boundary conditions from the global system PSY4: one field per day, horizontal resolution 1/12 ° x 1/12 °.

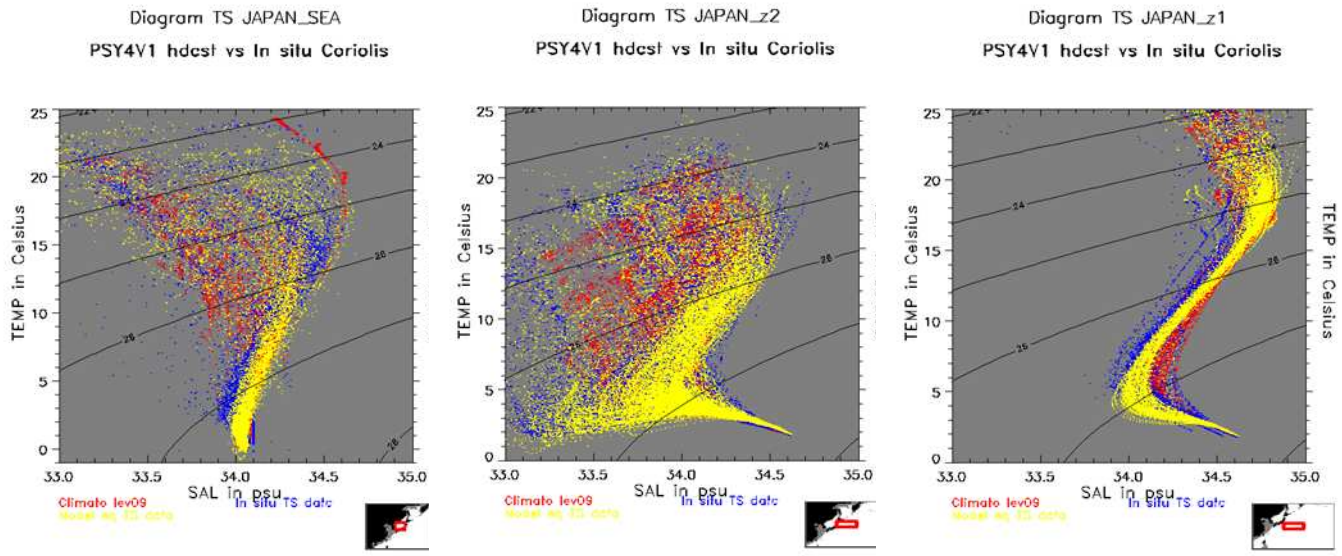

Figure 17 : Water masses (Theta, S) diagrams in the Japan Sea (left) and the regions North of Kuroshio (middle) and South of Kuroshio (right): comparison between PSY4V1R3 (yellow dots), Levitus WOA05 climatology (red dots) and Coriolis in situ observations (blue dots) in October-November-December 2011.

Three days after the Fukushima nuclear power plant accident, the International Atomic Energy Agency (IAEA) got in touch with the SIROCCO group to obtain information about the fate of radionuclides released by the power plant in the Japanese coastal waters. A 3D configuration of the SYMPHONIE model (Marsaleix et al., 2008, 2009) was rapidly implemented over the region. The numerical domain was built with two main concerns about the mesh size. The main idea was the necessity of high resolution near the power plant to represent at best the punctual release of radionuclides and then to describe correctly the alongshore dilution. Meanwhile this low resolution offered better opportunities of validation. Besides, for the sake of simplicity and rapidity, it was decided to choose a grid allowing to be directly embedded in the Mercator fields and then to get a mesh size at the lateral boundaries smaller but comparable to the Mercator one. These two constraints led us to choose a curvilinear grid with a grid mesh of 600 m at the power plant increasing up to 5 km at the boundaries.

Another point was to select appropriate bathymetry and tidal forcing. A bathymetry at 500 m resolution from the Japan Oceanographic Data Centre was used and then the T-UGO finite element model was implemented on a high resolution grid around Japan to provide an accurate tidal forcing to the 3D model.

Every week, the large scale forcing was received from Mercator. As soon as the SIROCCO server downloaded these forcing, the hydrodynamic high resolution simulation initialized in March 2011, a few days before the events, was then extended. In the same time, TEPCO, the operator of the power plant started on March 21 to sample daily the radionuclides concentration in the ocean, first near the outlets of the power plant and progressively at different sites around the power plant. The IAEA collected these data and transmitted them to SIROCCO as soon as they were available (one-day delay). Every week, several successive simulations of tracer dispersion were run in offline mode, progressively adjusting the source term of Cesium 137 to obtain a good agreement between the concentration measured and observed at the power plant.

The direct release of radionuclides issued from leakages or from the operations for reactors cooling were not the only inputs to the sea as important releases to the atmosphere were also introduced into the ocean through deposition. During a first period, we did not get any precise information about the amounts of radionuclides concerned by this transfer except some preliminary maps giving orders of magnitude transmitted by IAEA. The situation changed on mid-April when the CEREA laboratory (Ecole des Ponts ParisTech and EDF R&D) was able to provide results from the transport model Polyphemus/Polair3D previously validated on radionuclides dispersion events (Quélo et al., 2007). This model was driven by the ECMWF meteorological fields at a resolution of ¼° while the source term was estimated from the temporal profiles of the TEPCO gamma dose measurements on the power plant site (Winiarek et al., 2012). The hourly fields of Cesium deposition produced by this model were used as a second source of tracer for the SIROCCO dispersion model.

The results of the marine dispersion model were systematically compared to all the observations available. As already mentioned, the number of sampled sites was regularly increasing, requiring update of the routines. Their geographic position was often not given (only the name

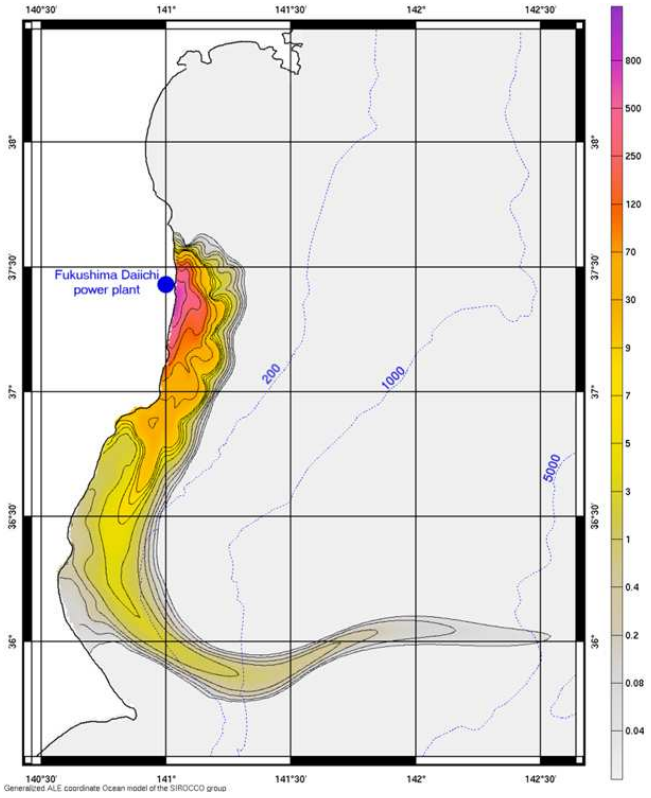

Figure 18 : Model Surface Concentration of Cesium 137 200110418

of the nearest city and sometimes with orthographic mistakes due to the translation from Japanese to English) making the job difficult. But finally, the results of the dispersion model as well as the validations were presented and renewed as often as possible on the SIROCCO website.

The SIROCCO group was the first one, ten days after the IAEA request, to publish on the web results of the marine dispersion of radionuclides. Clearly, this was made possible thanks to the efforts undertaken by the group to replace the time-consuming pre-processing of the forcing by online processing completely transparent for the users. No doubt that the national role (INSU Tâche de Service) of SIROCCO that consists to distribute and to train beginners to modelling played an important role in this choice.

Finally the modelling results were used to provide information about the regions impacted by the contamination and the duration of this contamination. The manual adjustment of the source term cited above was later improved through the use of an inverse method which provided the total amount of Cesium 137 (~4 Peta Becquerel) directly introduced into the sea (Figure 18). A paper describing the main results about the source term and the dispersion was recently submitted (Estournel et al., 2012).

The Lagrangian drift of water particles

For the MyOcean component of GMES, Mercator Ocean has calculated the Lagrangian drift of water particles from the analysis provided by the global ocean system PSY4 since March 12th, 2011. For that purpose, we coloured a set of water particles (used as tracers) near the Fukushima nuclear power plant between 0 and 30m deep, and we monitored their drift with a monthly update, as shown in Figure 19. This is done using the computational tool ARIANE (Blanke and. Raynaud, 1997). For each update we start from the water particle positions of the previous simulation.

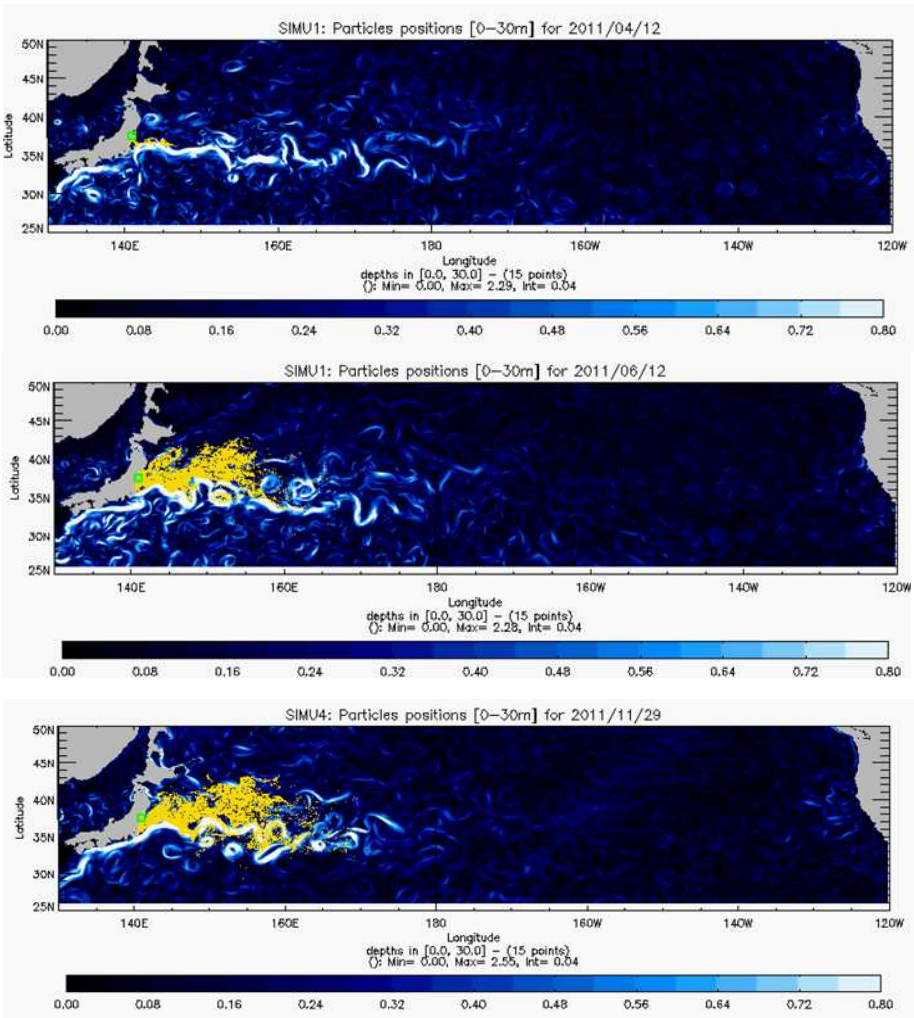

- We have calculated the Lagrangian drift of water particles from the analysis provided by the global ocean system since March 12th, 2011. For that purpose, we coloured a set of water particles (used as tracers) near the Fukushima nuclear power plant between 0 and 30m deep, and we monitored their drift with a monthly update, this is done using the computational tool ARIANE (Blanke and Raynaud, 1997). For each update we start from the water particle positions of the previous simulation.

- The green square represents the location of the Fukushima nuclear power plant. The yellow dots represent the coloured water particles. The simulation shows that, from the accident until August 31st, 2011, the coastal currents carry the coloured particles along the Kuroshio Current with dispersion towards the North of the current and East of the basin.

Figure 19 : Position of water particles after one (upper), three (middle) and 8.5 (lower) months of simulation.

At the date of 2001/11/29, the water particles continue to spread along the Kuroshio, reached 170 ° E. Their positions are mainly in the north of the Kuroshio front and the specific dynamic of the current with the both geostationary meanders, seems to slow down their progression eastward.

Weekly report offshore Japan

Since March 11 2011, date of the Fukushima nuclear disaster, Mercator Ocean has published on its website a weekly bulletin (Figure 20) commented and enhanced by scientific expertise on the situation of currents offshore Japan.

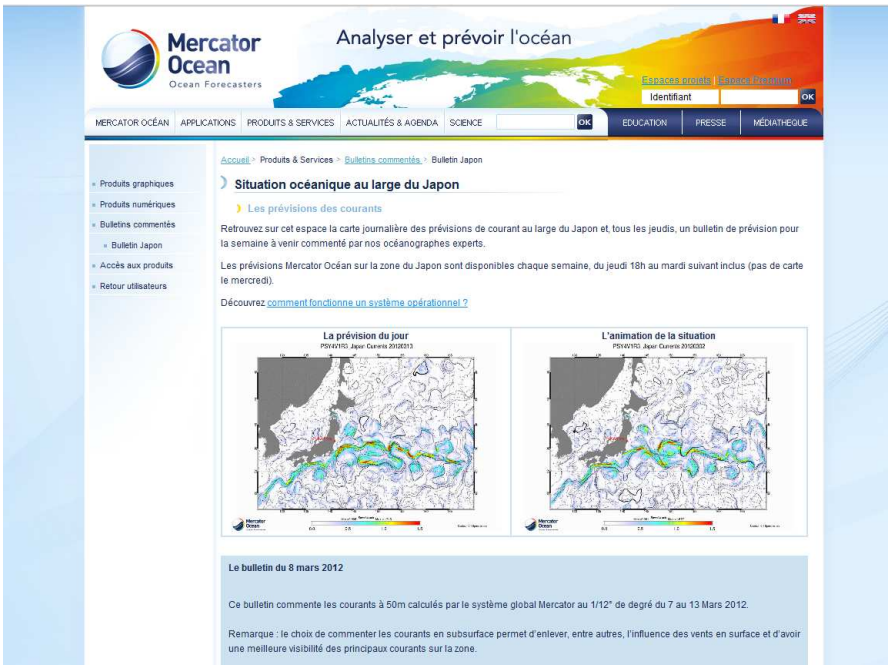

Figure 20: snapshot of Mercator web page dedicated to the weekly report.

Conclusion

The operational global ocean system PSY4V1 is robust and gives a good representation of the main physical processes of the whole ocean and particularly in the North Pacific Ocean with a good position of the main fronts: Kuroshio and Oyashio currents. The comparison of PSY4V1 velocity, temperature and salinity fields with observations offshore the Japanese coast gives good results. Mercator Océan has provided boundary conditions for the ocean circulation model SIROCCO of the Laboratory of Aerology to investigate the dispersion in seawater of radionuclides emitted by the Fukushima nuclear plant. Moreover Mercator Ocean has calculated the lagrangian drift of water particles from the analysis provided by the global ocean system PSY4 since March 12th, 2011, and published a weekly bulletin of the state of currents offshore the Japanese coast.

The main conclusion of this paper is the ability of the Mercator Océan global operational system PSY4V1 to provide in real-time specific information in a particular area, in the present case in the framework of the Fukushima disaster in the North Pacific Ocean.

References

Barnier B., Madec G., Penduff T., Molines J.-M. and 15 co-authors of the DRAKKAR Group, Impact of partial steps and momentum advection schemes in a global ocean circulation model at eddy permitting resolution, Ocean dynamics, 2006, doi:10.1007/s10236-006-0082-1.

Blanke, B., Raynaud S: Kinematics of the Pacific Equatorial Undercurrent: An Eulerian and Lagrangian approach from GCM results; JOURNAL OF PHYSICAL OCEANOGRAPHY Volume: 27 Issue: 6 Pages: 1038-1053; JUN 1997.

Drévillon M., Desportes, C., M., Régnier C., 2011 : QUO VA DIS (Quaterly Ocean Validation Display) #4 , #5.

Drillet, Y., Bricaud C., Bourdallé-Badie R., Derval C., Le Galloudec O., Garric G., Testut C.E., Tranchant B. : The Mercator Ocean Global 1/12° operational system : Demonstration phase in the MERSEA context ; Newsletter Mercator-Océan N°29, April 2008.

Estournel, C., Bosc, E., Bocquet, M., Ulses, C., Marsaleix, P., Winiarek, V., Osvath, I., Nguyen, C., Duhaut, T., Lyard, F., Michaud, H. and Auclair, F. Assessment of the amount of Cesium 137 released into the sea after the Fukushima accident and analysis of its dispersion in the Japanese coastal waters. 2012. Submitted.

Fichefet T. and Gaspar P., 1988. A model study of uppet ocean-sea ice interaction, J. Phys. Oceanogr. 18, 181-195

Goosse H, Campin J-M, Deleersnijder E, Fichefet T, Mathieu P-P, 2001: Description of the CLIO model version 3.0. Institut d'Astronomie et de Géophysique Georges Lemaitre, Catholic University of Louvain, Belgium.

Guinehut S., A.-L. Dhomps, G. Larnicol and P.-Y. Le Traon, 2012: High resolution 3D temperature and salinity fields derived from in situ and satellite observations. To be submitted to Ocean Science (MyOcean Special Issue).

Madec G., 2008.NEMO reference manual, ocean dynamics component. Note du pole de modélisation, IPSL France N°27 ISSN N°1288-1619.

Marsaleix P., Auclair F., Floor J. W., Herrmann M. J., Estournel C., Pairaud I., Ulses C., 2008. Energy conservation issues in sigma-coordinate free-surface ocean models. Ocean Modelling, 20, 61-89.

Marsaleix, P., Auclair, F. and Estournel, C., 2009. Low-order pressure gradient schemes in sigma coordinate models: The seamount test revisited. Ocean Modelling, 30, 169-177.

Piacentini A., Buis S., Declat D. and the PALM group, PALM, 2003. A computational Framework for assembling high performance computing applications,Concurrency and Computat.: Pract. Exper.,00,1-7.

Pham, D., Verron, J., and Roubaud, M., 1998. A Singular Evolutive Extended Kalman filter for data assimilation in oceanography. J. Mar. Syst., 16(3-4), 323-340.

Quélo, D., Krysta, M., Bocquet, M., Isnard, O., Minier, Y. and Sportisse B., 2007. Validation of the Polyphemus platform on the ETEX, Chernobyl and Algeciras cases. Atmos. Env., 41, 5300-5315.

Qiu, B., 2001. Kuroshio and Oyashio Current, 2001, *Academic Press*

Qiu, B., 2010. Effect of Decadal Kuroshio Extension Jet and Eddy Variability on the Modification of North Pacific Intermediate Water, Qiu and Chen, *Journal of Physical Oceanography*,

Winiarek, V., Bocquet, M., Saunier, O. and Mathieu, A., 2012. Estimation of errors in the inverse modeling of accidental release of atmospheric pollutant: Application to the reconstruction of the Cesium-137 and Iodine-131 source terms from the Fukushima Daiichi power plant. In revision for the Journal of Geophys, Res, Atmospheres, in press.

DRIFT FORECAST WITH MERCATOR OCEAN VELOCITY FIELDS AND ADDITION OF EXTERNAL WIND/WAVE CONTRIBUTION

By S. Law Chune [1], Y. Drillet[1], P. De Mey[2] and P. Daniel[3]

[1]*Mercator Océan, Toulouse, France*
[2]*LEGOS CNRS, Toulouse, France*
[3]*Previmar Météo France, Toulouse, France*

Introduction

Predicting the fate of sea pollutions or drifting objects is a crucial need during disasters and also a very challenging task for ocean models. In case of incident over the French marine territory, Météo France has the responsibility to provide reliable ocean drift forecasts for authorities and decision makers. For that purpose, the oil spill model MOTHY (Daniel et al, 1996) was developed and is operated on duty 24/7/365. This system quickly computes the top layer surface ocean's response to rapid changes in the atmospheric forcing to estimate surface trajectories, but provide limited forecasts in waters dominated by large scale currents or meso-scale features and eddies. Oceanographic operational systems are an efficient tool to have access to realistic surface currents, and since 2007, MOTHY is fed with currents forecasted by Mercator Océan's assimilated systems. This cooperation already provided helpful assistance in the past, like during the Prestige incident where forecasts in the Bay of Biscay were improved thanks to large scale currents supplied by operational oceanography, in particular by Mercator-Océan.

The first part of this paper focusses on the forecast error ranges obtained with several oceanic simulations used in the reproduction of surface buoys trajectories collected in two specific areas: the Western Mediterranean sea and the southern part of the Guinea Gulf along the Angola coast. Drift forecasts have been computed with the 1/12° oceanographic system operated by Mercator Océan (PSY2V3R1) (Dombrowsky et al, 2009) and with some regional nested configurations especially developed for this study to evaluate benefits of some modeling improvements. In a second part, we present a simple way to take into account the windage and the Stokes drift, the latter leading to a strong improvement of forecast in case of significant wind. The forecast period that we are interested in goes from a few hours up to three days, a typical timescale for a quick action when an incident occurs.

Oceanic simulations

The operational forecast system evaluated in this study is the high resolution 1/12° North Atlantic (between 20°S and 80°N) and Mediterranean Sea system called PSY2V3R1. This system leans on the NEMO ocean model (Madec, 2008) and is configured with a classical set of parameters and numerical schemes usually used in global ocean configurations (Barnier et al, 2006). Details about model options are available in Table 1. The along track altimetry observations, the insitu temperature and salinity profiles and the RTG sea surface temperature are assimilated through the SAM2 assimilation code derived from the SEEK filter (Tranchant et al, 2008). The surface currents are undoubtedly the most critical data for drift application and the assimilation of sea level anomaly strongly constrains this field with large and meso-scale observed features. In PSY2V3R1, the assimilated sea level anomaly products are smoothed in space and time such that smaller oceanic features (in the range of 10 km and under) are free. For the Mediterranean Sea the spatial filtering is 42 km, whereas it is larger in equatorial regions like the Angola area where it reaches 250 km.

The regional configurations developed for this study take advantage of new developments for high resolution regional modeling (Cailleau et al, 2010). They are embedded inside the operational PSY2V3 system (see Table 1). They are also declined in two horizontal resolutions (1/12° and 1/36°) and provide 3 h high frequency outputs when only daily outputs are available for PSY2V3. One year simulations have been produced for validation purpose over an annual cycle and sensitivity experiments have also been performed to evaluate separately the benefits of some of these new specificities (not discussed in this paper).

In this article, we will focus on the impact of the horizontal resolution refinement (1/12° vs 1/36°) and on the offline inclusion of external wind effects. The later encompass the direct drag of the wind on emerged parts called windage, and the Stokes drift which is the residual transport induced by the wave field (Phillips, 1977). The regional configurations have been designed to cover two case studies. The first one is in the Western Mediterranean Sea where a real condition experiment has taken place during winter 2007 and produced the trajectories of six satellite tracked surface drifters. The second one is in the southern part of the gulf of Guinea, along the Angola coast, in March 2008 where the Total petroleum society has provided us two trajectories of the same kind. The regional configurations therefore possess the generic names of MEDWEST12, MEDWEST36, ANGOLA12 and ANGOLA36. The drifters used in both experiments are buoys of PTR type, a specific material manufactured to reproduce oil behavior in sea and usually released by aircraft inside marine pollutions to track them.

	PSY2V3R1	MEDWEST and ANGOLA configurations
Vertical resolution	50 levels 1 m in surface, 450 m at bottom	Identical to PSY2V3
Bathymetry	Etopo 2007	Combined product of Gebco 2008 and Etopo 2009
Horizontal resolution	1/12°	1/12° and 1/36°
Surface boundary condition	Filtered free surface	Explicit free surface with time splitting
Tide	No	Astronomic potential and TPXO tide model data at the open boundaries
Vertical physic modeling	TKE	kε
Convection	Enhanced convection in case of instability	Took into account in the kε model
Advection scheme	TVD	Quickest-ultimate
Diffusion	Laplacian isopycnal	Horizontal bilaplacian
Viscosity	Horizontal bilaplacian	Horizontal bilaplacian
Lateral friction	Partial slip condition in Atlantic (shlat = 0.5) and no slip in Mediterranean sea	Partial slip condition everywhere except in Gibraltar strait where a no slip condition is applied
Atmospheric forcing	Daily forcing with CLIO bulk formulation (ECMWF operational analyses)	High frequency (3h) forcing with CLIO bulk formulation (ECMWF operational analyses)
Runoff	Climatological runoff as excess of precipitation (Dai and Trenberth)	Climatological runoff as open boundary condition (Dai and Trenberth)
Ocean boundaries	Relaxation area toward levitus climatology	Daily open boundaries from PSY2V3R1 system with a temporal filtering to remove assimilation jumps
Initial conditions	Levitus climatology	PSY2V3R1 analyzed state with 15 days of spin up
Assimilation scheme	SAM2 assimilating along track sea level anomaly, insitu temperature and salinity profiles and RTG sea surface temperature maps.	No data assimilation

Table1: main characteristics of the operational system (PSY2V3) and of the regional configurations (MEDWEST and ANGOLA) used in this study.

The MEDWEST configurations have been initialized on September 26 2007 and a three month simulation has been performed with the ECMWF operational atmospheric analysis surface forcing and the PSY2V3R1 ocean analysis input at open boundaries. The ANGOLA configurations have been initialized on 13 February 2008 with the same conditions for a shorter simulation as only one month of lagrangian observations was available in this area.

Trajectories forecasting

The velocities fields produced with these systems have been used to produce surface trajectories with MOTHY and another particle fate model named Ariane.

MOTHY computes the 3D trajectories of simulated particles transported by the surface layer currents and adds other specific effects like buoyancy and diffusivity in case of pollutant modelling. The ocean current estimation is computed through several steps. In a first step, a barotropic model forced by the wind and the atmospheric pressure produce a first estimate. In a second step, a vertical profile of the current

is diagnosed through a 1D eddy viscosity model. This approach only models the surface ocean fast response to wind and pressure, and a possible third step adds a background current with large and meso-scale oceanic features. In our case, this background current is one daily extraction at a diagnosed Ekman depth of the ocean currents provided by Mercator systems (the operational or the regional configurations) which is directly added to ocean current computed by Mothy. This operation ensures that the atmospheric forcing is not taken into account twice. For that study, the pollutant version of MOTHY was configured to work on a 1/12° of horizontal resolution grid and forced by ECWMF's 6h average analysed wind and pressure.

The second approach is to generate from the surface currents of our oceanic simulations direct surface trajectories. This work was done with the lagrangian offline tool Ariane (Blanke and Raynaud, 1997). This software takes as input files 3D or 2D velocities fields, but our work restricted to the computation of 2D surface drift. In that case, the first level available in the oceanic outputs is used (50 cm of depth) with a daily temporal forcing frequency for PSY2V3 and 3 h of temporal frequency for the regional configurations.

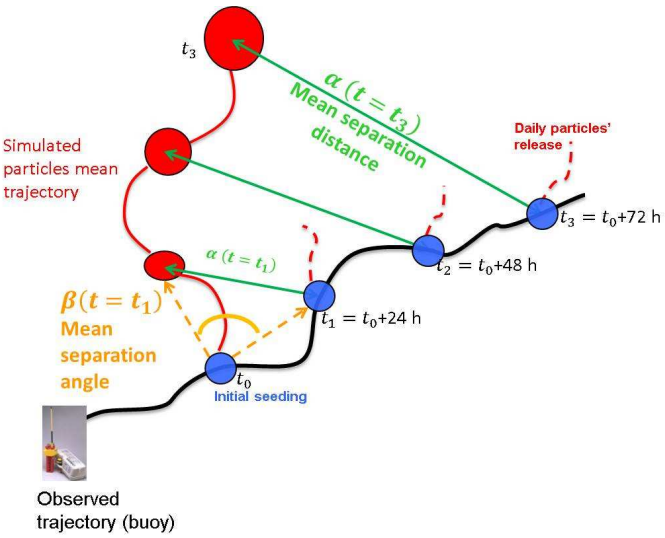

Figure 1: Protocol of the drift simulations. Simulated particles are seeded each 24 h along the observed drifter trajectory. Each seeding corresponds to a drift simulation which is performed during three days using Ariane or MOTHY and our ocean simulations. For each forecast, a distance error between the real position (black) and the forecasted mean trajectory of the particles (red) is computed. The green arrows represent the error in distance for one, two and three days of forecast. This distance error is evaluated along the forecast period.

Several drift predictions are performed from the lagrangian data (the observed trajectories) following the protocol described in Figure 1. A three day long trajectory is forecasted every day with an initialization of a set of particles situated around observed positions. For Ariane, the number and the distribution of particles for each forecast depend on the drifter's position uncertainty at the initialization point. This information is provided by the Argos system localization error classes. Usually, few hundreds of particles are used to simulate a buoy. For instance, a 1500 m uncertainty in the observed position unfolds from the seeding of 1200 particles. For MOTHY, this number is fixed to 480 particles systematically initialized right at the observed position. MOTHY's turbulent diffusion model which is parameterized with a random walk scheme formulation ensure a quick dispersion of particles during the forecast. In both cases, the mean trajectory of all of the virtual particles is retained to score the distance error by comparison with the real trajectory taken by the drifter.

Forecast errors in Angola

Figure 2 shows the trajectories of the two drifters collected off Angola and the corresponding forecasted segments of trajectories computed with the regional systems surface currents at 1/12° and 1/36° of horizontal resolution. The starting points of the buoys series are situated just southward of the Congo mouth (around 7°S and 12.5°E) with a day of delay between the two. The first buoy has a northward trajectory whereas the second shows a southward one, illustrating the reversal of currents occurring near the coast, likely due to interactions between wind, coastal trapped waves and the Congo River's plume. The modeled trajectories are not significantly different between the 1/12° and 1/36° forecasts. For both case, the northern part trajectories above 5°S show similar behavior with angle errors nearly at 90° to the observation. Around 5°S, the winding of trajectories are linked with inertial oscillations (visible in the observed trajectories) and are partially reproduced by the models. In the southern part of the domain, the southward coastal current around 8°S is nevertheless better represented at 1/36°, especially with a far better estimation of its offshore bifurcation due to the bathymetry at 9°S.

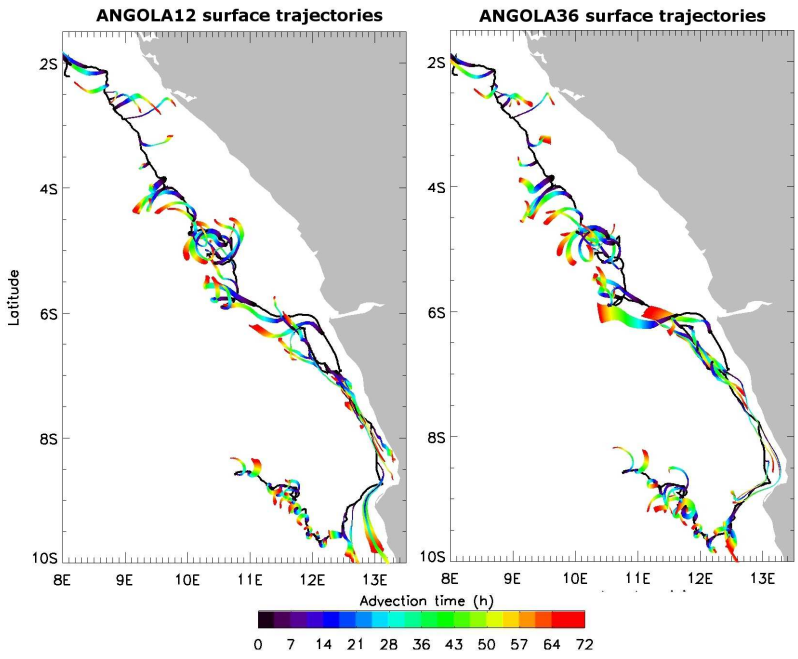

Figure 2: Observed and simulated trajectories with the regional configurations in the Angola area. The trajectories of the buoys are in black with an initial release situated at 7°S, 12.5°E. The positions of simulated particles with respected to time are coloured from 0 h (black) to 72 h (blue). The left panel shows the forecasts provided with the 1/12° configuration and the right panel the ones obtained with the 1/36° version.

The increase of the average distance error with time for the simulations made with Ariane forced by the surface currents available and with Mothy (supplied by ANGO-

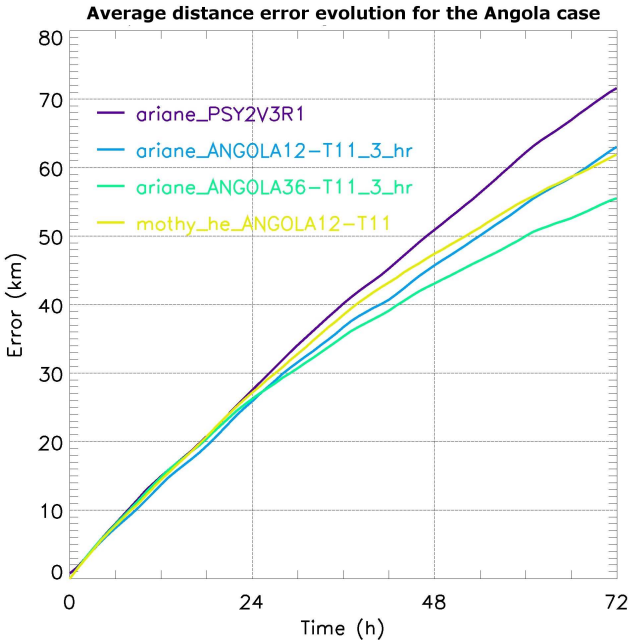

Figure 3 : Evolution of the mean distance error with respect to time for all forecasts performed in the Angola area. Ariane_PSY2V3, ariane_ANGOLA12-T11_3_hr, ariane_ANGOLA36-T11_3_hr are simulations obtained with the operational system PSY2V3 and the two regional systems surface currents forcing Ariane. Mothy_he_ANGOLA12-T11 is the simulation obtained with the MOTHY system and velocities field extracted from ANGOLA12 added in background.

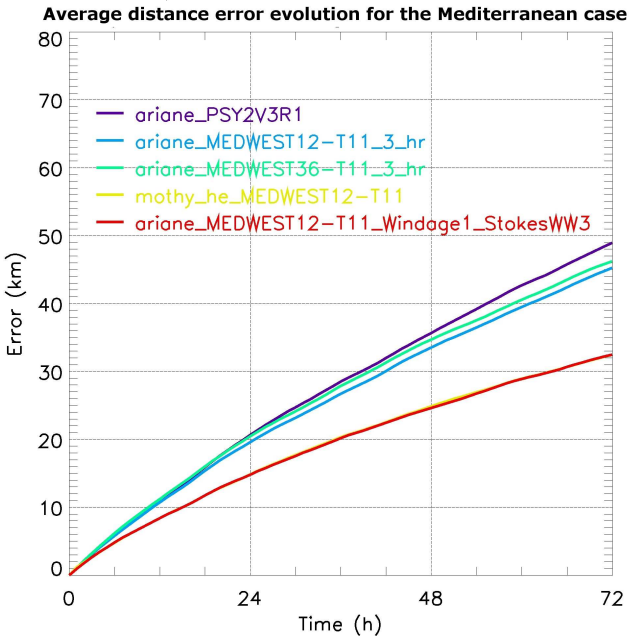

Figure 4 : Evolution of the mean distance error with respect to time for the Mediterranean case (same as figure 3). The supplementary red curve corresponds to the forecasts performed with MEDWEST12 added with a windage parameterization and the Stokes drift computed by WW3 wave model.

LA12) is presented in figure 3. The worst forecast is realized with the operational PSY2V3R1's surface currents with 26.4 km, 50 km and 71 km for the first, second and third day of integration. The use of regional 1/12° configuration decrease these errors to 25 km, 45 km and 62.3 km for the same forecast periods. The increase of the resolution (i.e. from 1/12° to 1/36°) leads to some benefit for mid and long term forecasts with 42.5 km and 55.1 km for the second and third day of integration, but provides in average slightly worse scores for forecasting time lower than one day. On that specific case, MOTHY's forecast are shown to be less efficient that the ones compute from the regional configuration's surface currents. This result is explained by the joint action of two facts. Firstly, the low wind situation often occurring during this period leads to very weak surface currents computed by Mothy. Those currents can't in any case represent the complex physic occurring near the Angola coast. Secondly and as consequence, a larger weight is given to the background current, but a strong baroclinicity make irrelevant the extraction of the velocity at the Ekman depth (~40 m), leading sometimes to contraflow forecasts.

Forecast errors in the Western Mediterranean Sea

For the Mediterranean Sea experiment, the six surface drifters involved were deployed in the vein of the Liguro Provençal Current (LPC) near the Azur Coast. During the first days of the experiment, all the buoys followed the slope current, a behavior well reproduced by the simulated particles as illustrated for a single drifter in Figure 5. In the vicinity of the Gulf of Lion, Mistral wind blasts events provoked the dispersion of the drifters. Four of them have kept following the slope and travelled downstream until the Balearic seas (not shown here). The two others took a southward direction crossing the Western Mediterranean Sea seaward. One has beached on Minorca after 3 weeks out at sea. Figure 5 refers to the last of these trajectories.

Figure 4 presents the evolution of the mean distance error obtained for the several oceanic simulations evaluated here. If the mean error during the LPC's transport stays below 10 km even for a 3 day forecast, the mean error for all the experimentd with the operational system PSY2V3R1 is 19.8 km, 35 km, and 48.4 km for one, two and three days of forecast. Using the regional configurations only produced a slight improvement of these values compared to the Angola case, with forecast errors about 18.9 km, 33 km and 44.8 km with the 1/12° regional system for the same forecast periods. Moreover, the resolution refinement did not conduct to any forecast improvement but a slight deterioration of results. This effect is caused by the generation of likely incorrect sub-mesoscale structures in the 1/36° velocity field, whereas these structures were not produced in the 1/12° version. For this Mediterranean case, the best forecasts are realized with Mothy with the MEDWEST12 addition, mainly thanks to its specific surface physics which quickly responds to wind. Nevertheless, a much larger improvement was obtained with Mercator-Océan's surface current when a windage parameterization and the Stokes drift effects were taken into account,

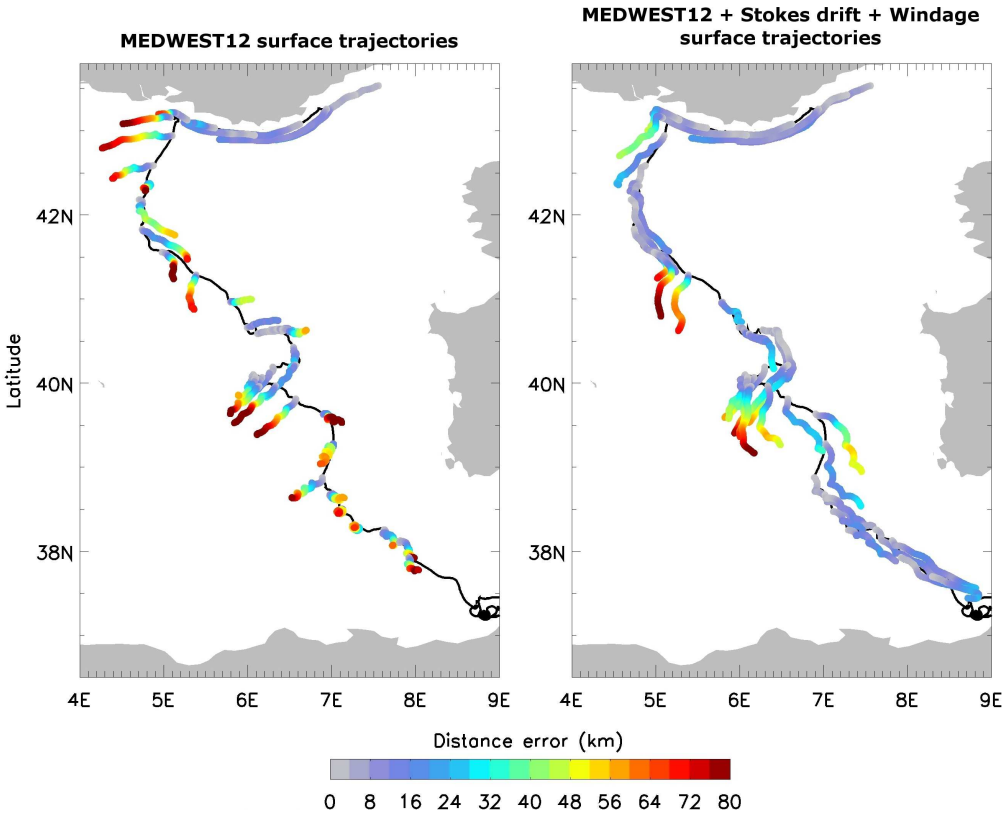

Figure 5:
Left: Average trajectories computed with the surface currents of the Mediterranean regional 1/12° configuration for one buoy (black). The forecasts are colored with respect to the distance error scored along time from 0 km (grey) to 80 km (red). Right: Same trajectories obtained with the addition of the windage and the Stokes drift.

especially because of winter wind condition. The addition of the latter processes gives errors of the same order of magnitude than MOTHY with MEDWEST12. The method and results are discussed below.

Complementary drift processes to the Mercator surface currents: windage and Stokes drift addition

The comparisons with Mothy and Mercator current profiles showed that the 1D analytic model used in Mothy for the vertical profile determination strongly react with respect to wind. In strong wind situation, it produces a relatively large surface velocity with a strong decay in the first meter. For the same wind, the velocity profile computed by the regional configurations is more mixed and submitted to a longer delay of response to wind changes. In order to investigate the missing physics in the surface current computed with NEMO, we have defined a very simple model of transport (equation 1) to include the windage and the Stokes drift, two processes that could contribute largely in case of significant wind situation.

$$U\_surf = U\_current + \alpha\_wind\ U\_10m + U\_wave$$

U_surf is the "total" surface current that will be used to perform the forecasts, U_current is the surface current provided by NEMO, α_wind U_10m is a percentage of the 10 meter wind speed (in this case we will take α_wind=1/100) and U_wave is the Stokes drift's velocity field. In this case Stokes velocities are directly provided by the WW3 wave model (Ardhuin et al, 2004) at 1/12° for the Mediterranean Sea and with a temporal frequency of 3 h.

Figure 5 illustrates the differences obtained for the trajectories computed offshore when only the surface current from the 1/12° regional system is used (left panel) and when this latter is completed with the additional terms of equation 1 (right panel). The improvement is clear all along the trajectory and particularly at the entrance of the Gulf of Lion during the wind event. The impact on the average error is large as shown on figure 4. The mean error decreases respectively to 15 km, 24 km and 32 km for the 1 day, 2 day and 3 day forecasts, which represents nearly 30% of improvement in comparison with the regional systems only for the three forecast ranges.

Conclusion

The main conclusions of this study is that an operational oceanic system based on primitive equations model like NEMO in realistic configuration and supplied with data assimilation is a useful tool to provide currents for drift forecast applications. Still, improvements are needed to decrease the forecast errors, the latter being in any case quite large for real case.

Developing regional configurations with a better physics has been seen to enhance the forecast in both cases. It also highlights the importance of understanding the specific ocean processes impacting surface drift, an analysis that can only be done through sensitivity experiments. For two studied areas, very different in term of dynamics, we have quantified the forecast errors for time range up to three days. It appears with our data set that the error is nearly 20% smaller for the Mediterranean Sea than for the Angola area. The robustness of these values is not completely acquired and other experiments over other seasons, dynamic regimes and with much more observations will be desirable.

The increase of the resolution showed a positive impact for the Angola case, but slightly degrades the results for the Mediterranean scenario. This result is not intuitive as the first Rossby radius is largely smaller in Mediterranean Sea that in tropical areas, so that a refinement of resolution would suggest a more accurate estimation of the velocity field features. Even if a good meso-scale (or smaller scale) representation is necessary for a good drift forecast, the actual precision of the operational systems which assimilate observations is still not sufficient for shorter scales. Improvements in small scale constraint through data assimilation are necessary for this kind of application and require higher resolution observations.

Nevertheless, some improvements are possible regarding physical processes, particularly when those one are not taken into account, like shown in that paper for a simple parameterization of the windage and the Stokes drift. This kind of improvement can also be adjusted in the ocean model through parameterization of the vertical mixing scheme or the computation of the wind stress (as shown by Mothy) or better, thanks to a dynamical coupling or a forcing of the ocean model with an external wave model.

Acknowledgements

The authors wish to thank the Midi Pyrenées Regional Council and Météo France that co-funded this study. This work has been realized in the framework of a PHd Thesis within the scope of a scientific collaboration between Meteo France, Mercator Océan and CNRS/LEGOS : “Contribution of operational oceanography to drift forecast for search and rescue operations and marine pollution response.” (Law Chune, 2012).

References

Ardhuin, F., Martin-Lauzer, F. R., Chapron, B., Craneguy, P., Girard-Ardhuin, F. and Elfouhaily, T. 2004 : Dérive à la surface de l’océan sous l’effet des vagues, C.R. Géoscience 366.

Barnier, B. Madec, G. Penduff, T. Molines, J.M. Treguier, A.M. Le Sommer, J. Bekmann, A. Biastoch, A. Boning, C. Dengg, J. Derval, C. Durand, E. Gulev, S. Remy, E. Talandier, C. Theeten, S. Maltrud, M. McClean, J. De Cuevas, B. 2006 : Impact of partial steps and momentum advection schemes in a global ocean circulation model at eddy-permitting resolution. Ocean dynamics. Volume 56, Numbers 5-6, pp. 543-567 (25)

Blanke B. and Raynaud S., 1997 : Kinematics of the pacific equatorial undercurrent: An eulerian and lagrangian approach from gcm results, J. Phys. Oceanogr. 27, 038–1053.

Cailleau, S., Chanut, J., Levier, B., Maraldi, C., Reffray, G., 2010 : The new regional generation of Mercator Ocean system in the Iberian Biscay Irish (IBI) area, Mercator Ocean Quarterly Newsletter#39 , pp 5-15.

Daniel P., 1996 : Operational forecasting of oil spill drift at météo-france, Spill Science and Technology Bulletin 3, 53–64.

Dombrowsky, E., Bertino, L., Brassington, G.B., Chassignet, E.P., Davidson, F., Hurlburt, H.E., Kamachi, M., Lee, T., Martin, M.J., Mei, S., and Tonani., M., 2009 : GODAE systems in operation. Oceanography 22(3):80–95, doi:10.5670/oceanog.2009.68.

Phillips O.M : The dynamics of the upper ocean, Cambridge University Press, London, 1977.

Law Chune S., 2012 : Apport de l’océanographie opérationnelle à l’amélioration de la prévision de la dérive océanique dans le cadre d’opération de recherché et de sauvetage en mer et de lutte contre les pollutions marines. Thèse de Doctorat. Université Paul Sabatier Toulouse

Madec G. 2008: "NEMO ocean engine". Note du Pole de modélisation, Institut Pierre-Simon Laplace (IPSL), France, No 27 ISSN No 1288-1619.

Tranchant B., Testut C.E., Renault L. and Ferry N., Obligis E., Boone C. and Larnicol G., 2008 : Data assimilation of simulated SSS SMOS products in an ocean forecasting system, Journal of operational Oceanography, Vol. 2008, No 2, pp 19-27(9).

GLORYS2V1 GLOBAL OCEAN REANALYSIS OF THE ALTIMETRIC ERA (1993-2009) AT MESO SCALE

By N. Ferry[1], L. Parent[1], G. Garric[1], C. Bricaud[1], C-E. Testut[1], O. Le Galloudec[1], J-M. Lellouche[1], M. Drévillon[1], E. Greiner[2], B. Barnier[3], J-M. Molines[3], N. Jourdain[3], S. Guinehut[2], C. Cabanes[4], L. Zawadzki[1].

[1] *Mercator-Océan, Ramonville St Agne, France*
[2] *CLS, Ramonville St Agne, France*
[3] *MEOM-LEGI, Grenoble France*
[4] *Coriolis, Plouzané, France*

Abstract

We present GLORYS2V1 global ocean and sea-ice eddy permitting reanalysis over the altimetric era (1993-2009). This reanalysis is based on an ocean and sea-ice general circulation model at ¼° horizontal resolution assimilating sea surface temperature, in situ profiles of temperature and salinity and along-track sea level anomaly observations. The reanalysis has been produced along with a reference simulation called MJM95 which allows evaluating the benefits of the data assimilation. We first describe GLORYS2V1 reanalysis system, and its main improvements with respect to the previous stream GLORYS1V1 which covered the Argo years (2002-2009). Then, the reanalysis skill is presented. Data assimilation diagnostics reveal that the reanalysis is stable all along the time period, with however an improved skill when Argo observation network establishes. GLORYS2V1 captures well climate signals and trends and describes meso-scale variability in a realistic manner.

Introduction

Describing the ocean state over the past decades to better understand the ocean variability is a great challenge and is the objective of ocean reanalyses. They have many downstream applications, the most known one being the climate monitoring and the use of ocean reanalyses as initial conditions for coupled ocean atmosphere monthly to decadal hindcasts. Reanalyses are also used for research studies as they provide a realistic (i.e. close to the observations) description of the full (all physical variables, gap free) ocean state. Reanalyses may also be used as boundary conditions for regional ocean model configurations or as physical forcing for ocean biogeochemical modelling.

In the atmosphere, it is known for a long time that eddies (i.e. storms) actively participate to the transport of energy, especially at mid-latitudes (e.g. Vonder Haar and Ort, 1973). In the ocean, the amount of energy transported by eddies is less well known even though studies based on observations (e.g. Souza et al., 2011) or models (e.g. Smith et al. 2000) show that the eddies seem to have a significant contribution on the meridional heat transport. There is also evidence that ocean meso scale features have an impact on the atmospheric winds (e.g. Chelton et al., 2004, Maloney et al., 2006). That is why, including meso scale feature in ocean reanalyses is an important issue and contributes to improve our understanding of ocean and climatevariability.

Mercator, the French ocean analysis and forecasting centre, the Drakkar consortium (Drakkar Group, 2007) and Coriolis data centre have put together their expertise to develop a global ocean eddy permitting resolution (1/4°) reanalysis system. This work has been done in the framework of the French GLobal Ocean ReanalYsis and Simulations (GLORYS) and the EU funded MyOcean projects. The objective is to produce a series of realistic (i.e. close to the existing observations and consistent with the physical ocean) eddy resolving global ocean reanalyses. A first reanalysis called GLORYS1V1, spanning the 2002-2008 time period (the “Argo” era) was produced and is described in Ferry et al. (2010). GLORYS1V1 was considered as a benchmark and the results over this well observed time period showed that the reanalysis system performed quite well. Producing skilful eddy permitting global ocean reanalyses starting before Argo era (i.e. before 2001) is still a big challenge, mainly because in situ temperature and salinity observations are very scarce in space and time.

We present in this study GLORYS2V1 17-year long reanalysis spanning the altimetric era (1993-2009) along with MJM95 reference simulation where no data were assimilated. This reanalysis benefits from several improvements compared to its predecessor GLORYS1V1. The main novelties are (i) a new sea-ice ocean model configuration ORCA025 with 75 vertical levels forced with ERA-Interim 3H surface atmospheric parameters, (ii) a 3D-Var bias correction scheme for temperature and salinity and (iii) updated quality controlled delayed time (DT) observations used for data assimilation. The differences between GLORYS1V1 and GLORYS2V1 reanalysis systems are summarized in Table 1.

The details of the improvements of GLORYS2V1 reanalysis configuration are detailed in the first three sections of the paper, devoted respectively to (i) the model configuration, (ii) the data assimilation method and (iii) the assimilated observations. Then, various validation diagnostics are presented, showing that GLORYS2V1 has an overall good skill in simulating the ocean during the altimetric era. A summary and conclusions section ends this paper.

The model configuration

The ocean/sea ice model is the free surface, primitive equation ocean general circulation model from the NEMO numerical framework (version 3.1, Madec, 2008) and has many common features with the ORCA025 model developed by the European DRAKKAR consortium

	GLORYS1V1	GLORYS2V1	MJM95
NEMO code	NEMO1.09, LIM2_EVP	NEMO3.2, LIM2_EVP	NEMO3.2, LIM2_EVP
ORCA025 configuration	50 levels	75 levels	75 levels
Surface forcing	ECMWF, daily aver., oper., CLIO bulk	ERA-Interim, 3H turbulent fluxes, CORE bulk, SW and LW daily aver. + corrections based on GEWEX, precip daily	ERA-Interim, 3H turbulent fluxes, CORE bulk, SW and LW daily aver. + corrections based on GEWEX, precip daily + SSS restoring (τ=60 days/10m)
Data assimilation method	Reduced order Kalman filter (SEEK formulation)	Reduced order Kalman filter (SEEK formulation) + 3D-Var bias correction scheme for T & S	None
Assimilated observations	SST, SLA+MDT, in situ T,S	SST, SLA+MDT, in situ T,S	None
SST	NCEP RTG0.5° SST	NOAA NCDC OI 0.25°	-
SLA	DT Aviso along-track SLA	DT Aviso along-track SLA	-
MDT	Rio et al., 2004	CNES-CLS09 + modif.	-
In situ T, S	CORA-2	CORA-3	-

Table 1: Main differences between GLORYS1V1 and GLORYS2V1 reanalysis configurations.

(Drakkar group, 2007), the numerical details of which are given in Barnier et al. (2006). The ¼° horizontal grid is defined as a generic tripolar 'ORCA' type mesh (Madec and Imbard, 1996) ranging from 3km resolution in the Canadian Archipelago to 28km at the equator. The geographical domain extends from 77°S to the North Pole. The bathymetry is the combination of the 1-nm bathymetry file (ETOPO2) of NGDC from Smith and Sandwell (1997) for the deep ocean below 300m depth and the GEBCO 1-nm bathymetry for the shelves (above 300m depth). The 75 vertical levels grid ranging from 1m at the surface to 200m at the bottom uses partial cells parameterization for a better representation of the topographic floor. Compared to the 50 levels used in the GLORYS1V1 configuration, the grid is still stretched at the surface (22 levels in the first 100m depth), extra levels are located principally in the thermocline layers ending to a 20m vertical resolution at the 200m depth and in the bottom layers where the coarsest resolution reaches 200m at 5000m depth. The sea ice component is the LIM2 thermodynamic-dynamic sea-ice model (Fichefet and Maqueda, 1997). Following options are implemented in the model configurations: the momentum advection term is computed with the energy and enstrophy conserving scheme proposed by Arakawa and Lamb (1981), the advection of the tracers (temperature and salinity) is computed with a total variance diminishing (TVD) advection scheme, a free surface filtering out the high frequency gravity waves is used (Roullet and Madec, 2000), a laplacian lateral isopycnal diffusion on tracers (300 m^2s^{-1}), an horizontal biharmonic viscosity for momentum (-1.10^{11} m^4s^{-1}). The vertical mixing is parameterized according to a turbulent closure model (order 1.5). Barotropic mixing due to tidal currents in the semi-enclosed Indonesian throughflow region has been parameterized following Koch-Larrouy et al. (2008). The lateral friction condition is a partial-slip condition. The Elastic-Viscous-Plastic rheology formulation for the LIM2 ice model (hereafter called LIM2_EVP) has been activated (Hunke and Dukowicz, 1997) together with a refreshing and spatially smoothed ocean-sea ice stress computation at each oceanic time step.

The monthly runoff climatology is built from coastal runoffs and 100 major rivers from Dai and Trenberth (2002) together with an annual estimation of the Antarctica ice sheets melting given by Jacobs et al. (1992). One third of this annual estimation is spread zonally in the open ocean until the 60°S latitude. This may represent freshwater input from melting icebergs. Atmospheric forcing fields are issued from the ERA-Interim reanalysis project (Dee et al., 2011). We use a 3 hours sampling to reproduce the diurnal cycle, concomitant to the use of the 1m thickness of the uppermost level and according to Bernie et al. (2005), this temporal and vertical resolution are sufficient to capture 90% of the SST diurnal variability and the maximum heating rates of the diurnal cycle. Momentum and heat turbulent surface fluxes are computed from bulk formulae (Large and Yeager, 2004) using the usual set of atmospheric variables: surface air temperature at 2m height, surface humidity at 2m height, mean sea level pressure and the wind at 10m height. Daily downward longwave (LW) and shortwave (SW) radiative fluxes and rainfalls (solid + liquid) fluxes are also used in the surface heat and freshwater budgets. An analytical formulation (Bernie et al., 2005) is applied to the shortwave flux in order to reproduce ideally the diurnal cycle. Representation errors of the ERA-Interim clouds (Dee et al., 2011) induce large errors in both radiative and rainfalls fluxes. We have applied a method to correct these large scale radiative fluxes biases (Garric et al., 2011) towards the Gewex (Global Energy and Water cycle Experiment; http://www.gewex.org/) project of the World Climate Research Program (WCRP). This correction is applied locally and modifies only the large scale. The interannual signal of the corrected flux is not modified as well as the synoptic events (such as cyclones). Moreover, this method can be applied outside the period of the satellite period. No attempt has been made to correct the ERA-Interim rainfall fluxes, consecutively the freshwater budget is far from being equilibrated. In order to avoid any mean sea surface height drift and to reduce errors in the SLA assimilation, the surface mass budget is set to zero at each time step with a superimposed seasonal cycle. We have implemented a 3D (Temperature, Salinity) restoring towards Gouretski and Koltermann (2004) dataset in the Southern ocean (southward 60°S) and under 2000m depth to stabilize the mass adjustment and the Antarctica

Circumpolar Current transport (Drakkar group, 2007). No newtonian surface damping is implemented. Following Lupkes (2010), we have cooled the warm ERA-Interim surface air temperature by 2°C and dry the surface humidity by 15% over sea ice and northward 80°N. Similarly, and despite the correction of the SW and LW fluxes, hindcasts experiments performed without data assimilation revealed an underestimation of the Antarctica sea ice extent during summer. To avoid this, we arbitrarily decreased by 20% the downward SW flux southward of 65°S. Erroneously, a gain of 10% in the LW flux component has been applied southward 65°S.

Temperatures and salinities are initialized with climatological fields from Levitus (1998) and ocean at rest. Sea ice fraction is issued from the mean December 1991 NSIDC satellite dataset (Comiso et al., 2008). Sea ice thickness is built from analytical relationships between sea ice fraction and sea ice thickness. The method is the following: the domains of the Arctic Ocean and Antarctica are decomposed into several sub-domains. For each sub-domain, an analytical function (usually a polynomial function of degree 3) is obtained by regression between the sea ice thickness and the sea ice fraction of the experiment, here the mean January of GLORYS1V1 over the 2002-2008 periods. The regressive coefficients are then applied (for each sub-domain) on the mean December 1991 NSIDC satellite data in order to obtaining the regressed sea ice thickness.

Data assimilation method

The data assimilation method relies on a reduced order Kalman filter based on the SEEK formulation introduced by Pham et al. (1998) and implemented in a realistic framework by Testut et al. (2003). This approach is used for several years at Mercator and has been implemented in different ocean model configurations. Here we present a short description of what we call Système d'Assimilation Mercator version 2 (SAM2). We present (i) the variant of the SEEK filter developed at Mercator, (ii) the 3D-Var temperature and salinity bias correction scheme used and (iii) the model initialization procedure. An important difference of GLORYS2V1 reanalysis system with classical analysis and forecasting systems is that the analysis time is not at the end of the assimilation window but at the middle of the 7-day assimilation cycle. The objective is to take into account information both in the past and in the future and to provide the best estimate of the ocean centered in time. Using such an approach, the analysis has a smoother like feature.

The Forecast error covariance

The SEEK formulation requires knowledge of the forecast error covariance of the control vector. This vector is composed of the 2D barotropic height, the 3D temperature, salinity, zonal and meridional velocity fields. The forecast error covariance is based on the statistics of a collection of 3D ocean state anomalies (typically a few hundred) and is seasonally variable (i.e. fixed basis, seasonally variable). This approach comes from the concept of statistical ensembles where an ensemble of anomalies is representative of the error covariances. With this approach the truncation does not take place any more, thus it is only necessary to generate the appropriate number of anomalies. This approach is similar to the Ensemble optimal interpolation (EnOI) developed by Oke et al., (2008) which is an approximation to the EnKF that uses a stationary ensemble to define background error covariances. In our case, the anomalies are high pass filtered ocean states (Hanning filter, length cut-off frequency = 1/30 $days^{-1}$) available over the 1993-2009 time period every 3 day. These ocean states come from a reference simulation carried out with the same ocean model configuration called MJM91, but without any surface salinity restoring towards climatology.

In summary, the covariance is estimated from the statistics of 120days/6days×16years = 320 ocean state anomalies and an adaptive scheme for the model error variance has been implemented which calculates an optimal variance of the model error based on a statistical test formulated by Talagrand (1998).

The Bias correction:

A bias correction scheme has been implemented in order to correct temperature and salinity biases when enough observations are present. The bias correction will correct the large scale slowly varying error of the model whereas the SEEK filter will correct the smaller scales of the model forecast error. It uses the information contained in the temperature and salinity innovations collected during the past three months. Then, a 3D-VAR method is used to analyze the bias. The bias covariance is constrained by the 3 dimensional density gradients in the ocean, i.e. the bias covariance has a smaller scale correlation scale in the vicinity of a front than away from this front. The algorithm is tuned to avoid any correction close to the main thermocline in order not to destroy its vertical gradient. Finally, these corrections are applied as tendencies (analyzed bias divided by a time scale τ, with τ=3months) in the model prognostic equations.

Figure 1 shows the positive impact of the bias correction on the global innovation RMS of temperature and salinity. Two experiments have been performed, one with and the other without the bias correction over a 15-month long hindcast performed with GLORYS2V1. In the experiment without bias corrections, large innovations RMS are present below 200m depth for temperature and below 600m depth for salinity (Fig. 1a and 1c). In the experiment with the bias correction scheme (Fig. 1b and 1d), the temperature bias located at 200-700m depth is largely reduced after 3 months of integration. In the deeper ocean (600-2000m), the same behavior is observed for the salinity field. The residual bias is mainly located at the bottom of the thermocline, where the bias correction does not act.

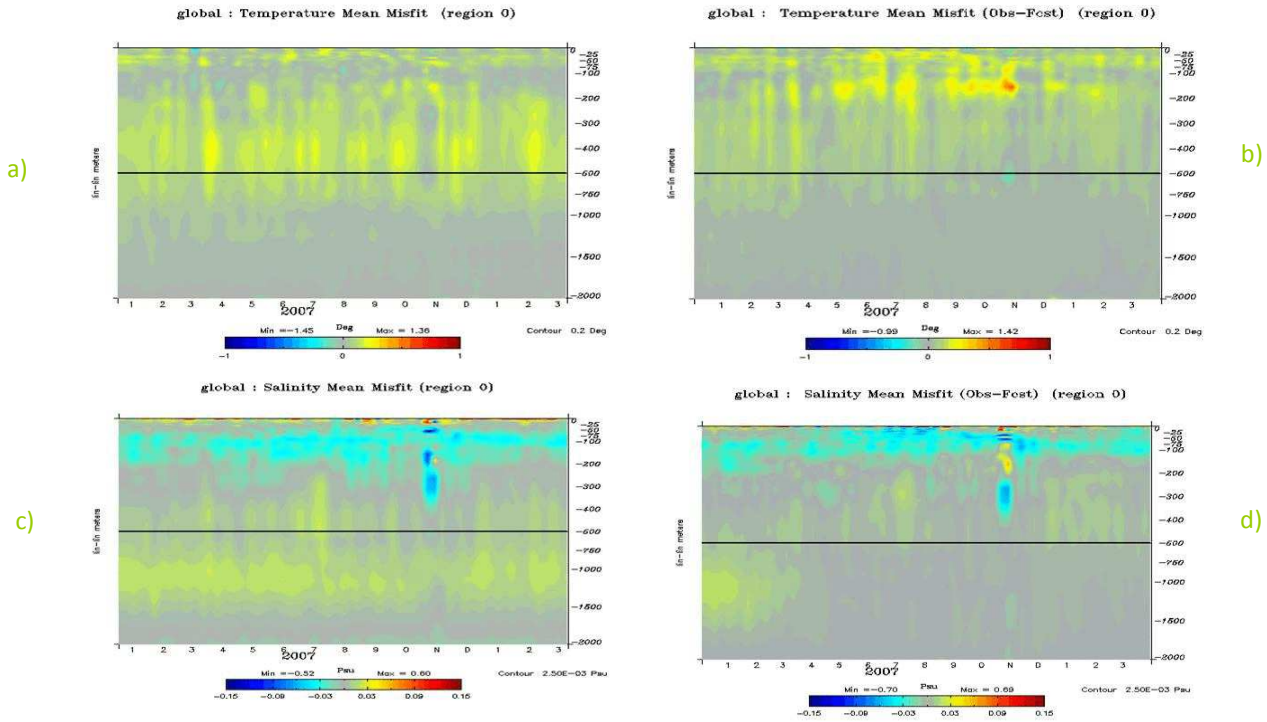

Figure 1: Temperature (a, b) and salinity (c, d) innovation (observation - background) RMS in two 15-month long global ocean hindcasts performed with GLORYS2V1. First experiment is without any bias correction (a, c) and second experiment is with a bias correction scheme (b, d). Units are degree Celsius for temperature and PSU for salinity.

The model initialization

The data assimilation produces after each analysis global ocean barotropic height, temperature, salinity and zonal and meridional velocity increments. A physical balance operator allows deducing from these increments a physically consistent sea surface height increment. These increments are then applied using an Incremental Analysis Update (IAU) method (Bloom et al., 1996, Benkiran and Greiner, 2008). In the variant of the IAU used at Mercator, the model integration over the assimilation window is performed a second time with the increments applied with the IAU technique. This allows reducing the spin up effects and it ensures the analyzed model trajectory to be continuous.

Assimilated observations

The assimilated observations consist in sea surface temperature (SST) maps, along track sea level anomaly (SLA) data, and in situ temperature and salinity profiles.

The SST comes from the daily NOAA Reynolds 0.25° AVHRR-only product (Reynolds et al., 2007) and is assimilated once per week at the analysis time (day 4 of the assimilation window). This SST product contains more mesoscale features than the NCEP RTG 0.5° SST product assimilated in GLORYS1V1 and one expects Reynolds 0.25° AVHRR-only product to provide complimentary information of meso scale signal to along track SLA. The DT along-track SLA data are provided by AVISO (SSALTO/DUACS Handbook, 2009) and benefit from improved DT corrections. The various altimetric satellite data assimilated in GLORYS2V1 come from Topex/Poseidon, ERS-1/2, GFO, Envisat and Jason-1/2. Table 2 synthesizes the altimetric data time coverage of each satellite. The assimilation of SLA observations requires the knowledge of a Mean Dynamic Topography (MDT). The mean surface reference used is CNES-CLS09 product (Rio et al., 2011) combined with a model mean sea surface height near the coasts. In situ temperature and salinity profiles come from the CORA-3 in situ data base provided by CORIOLIS data centre and available through MyOcean service (http://www.myocean.eu/). This in situ data base includes profiles originating from the NODC data base, from the GTS, from national and international oceanographic cruises (e.g. WOCE), from ICES data base, TAO/TRITON and PIRATA mooring arrays, and Argo array. The temperature and salinity profiles have been checked through objective quality controls but also visual quality check. Following the first quality check done by CORIOLIS data centre, additional quality check and data thinning is performed.

For each data set, an observation error including both the instrumental error and the model representativeness error (these two errors being supposed to be uncorrelated) are specified. The SST error is spatially variable with a minimum error equal to $(0.6° C)^2$. In the regions of large eddy variability the error is larger and can reach $(1.5 °C)^2$. The SLA observation error is specified according to the knowledge of the satellite accuracy and to the model representativeness error. So, we use a $(2 cm)^2$ instrumental error variance for JASON-1 and TOPEX-Poseidon and a $(3.5 cm)^2$ error for ERS-2, GFO and ENVISAT. For in situ temperature and salinity profiles, the error depends on the geographical location and

depth. For temperature, this error is dominated by the inaccuracy of the thermocline position given by the model and the data whereas for salinity, largest errors are located near the surface.

Time	1992	1993	1994	1995	1996	1997	1998	1999	2000	2001	2002	2003	2004	2005	2006	2007	2008	2009
Jason-2																	■	■
Jason-1N																	■	■
Jason1											■	■	■	■	■	■	■	
GFO									■	■	■	■	■	■	■	■	■	
Envisat												■	■	■	■	■	■	■
ERS-1		■	■	■	■	■	■	■	■	■	■							
ERS-2		■	■	■	■	■	■	■	■	■	■							
TPX-N												■	■	■				
TPX		■	■	■	■	■	■	■	■	■	■							

Table 2: Time period during which altimetric data sets are available. Jason-1N means Jason-1 new orbit. TPX means Topex-Poseidon. TPX-N means Topex-Poseidon new orbit. There is no ERS-1 data between December 23, 1993 and April 10, 1994 (ERS-1 phase D – 2nd ice phase).

Results of the reanalysis over the Altimetric period: 1992 - 2009

Here we present the results of GLORYS2V1 1992-2009 reanalysis. Assimilation diagnostics are first presented and reveal that the reanalysis system is stable and well constrained by the assimilated observations. Then, several large scale validation diagnostics of GLORYS2V1 are shown.

Assimilation diagnostics

We present in this section data assimilation diagnostics for SLA, SST and in situ temperature and salinity assimilated observations.
The mean and the RMS of SLA innovation for the global ocean are presented in Figure 2. The RMS of the misfit (innovation) is steady all along the reanalysis, less than 7cm RMS on average. The global average innovation is close to zero during the 17-year reanalysis, indicating that GLORYS2V1 is well reproducing the global mean sea level variations. This is consistent with the good agreement between observed (i.e. altimetric) and reanalyzed global mean SLA trends (not shown), indicating that GLORYS2V1 reproduces well the global sea level rise.

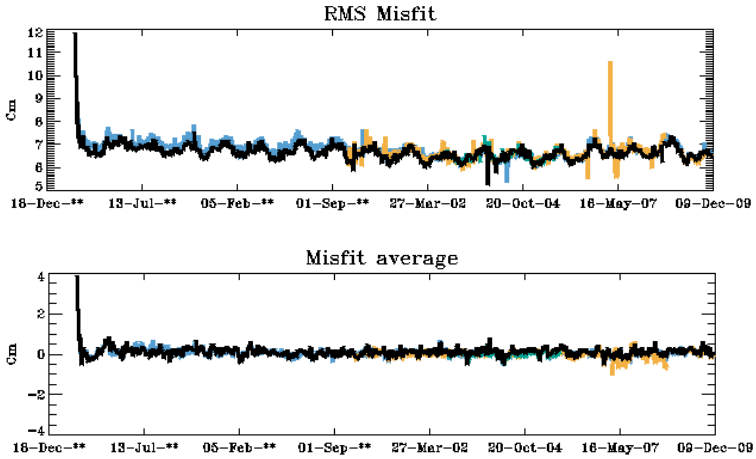

Figure 2: Data assimilation diagnostics for SLA for the global ocean from December 1992 until December 2009. SLA innovation RMS (a) and mean (b).

The assimilation of SST observations helps constraining the model upper layer temperature. Figure 3 represents the SST innovation RMS and average for the global ocean.

The assimilated SST product includes some meso-scale features and has a resolution similar to the model, so we can expect a better control of the surface layer and might have a better agreement between the ocean and the atmosphere dynamics. The innovation RMS is about 0.6-0.8°C all along the time period and exhibits seasonal signal amplitude of 0.1-0.2°C. The same innovation diagnostic using the in situ temperature profile observations close to the surface (depth < 5m) exhibits some similar features. The global average of the near surface in situ temperature innovation is close to zero, and the SST innovation RMS shows the same seasonal variations. During the 2004-2009 time period, the comparison with NCEP RTG0.5° (used only for diagnostic purposes) shows the same behavior and the same seasonal variations both for the mean and RMS, suggesting that the seasonal variations in the RMS is rather related to seasonally varying biases.

Lastly, we present data assimilation diagnostics for temperature innovations over the global ocean. Innovations statistics are shown in 4 layers ([0-100m], [100-300m], [300-800m], [800-2000m]) (Fig. 4a and 4b). A general comment is that there is a clear dependence of the reanalysis skill to the observation network. Before Argo era (2001-2009), the innovation RMS is larger (and noisier) than during the last decade. The curves of the mean innovation as a function of time are noisy (ocean is sampled irregularly in space and time) and are weakly biased. When

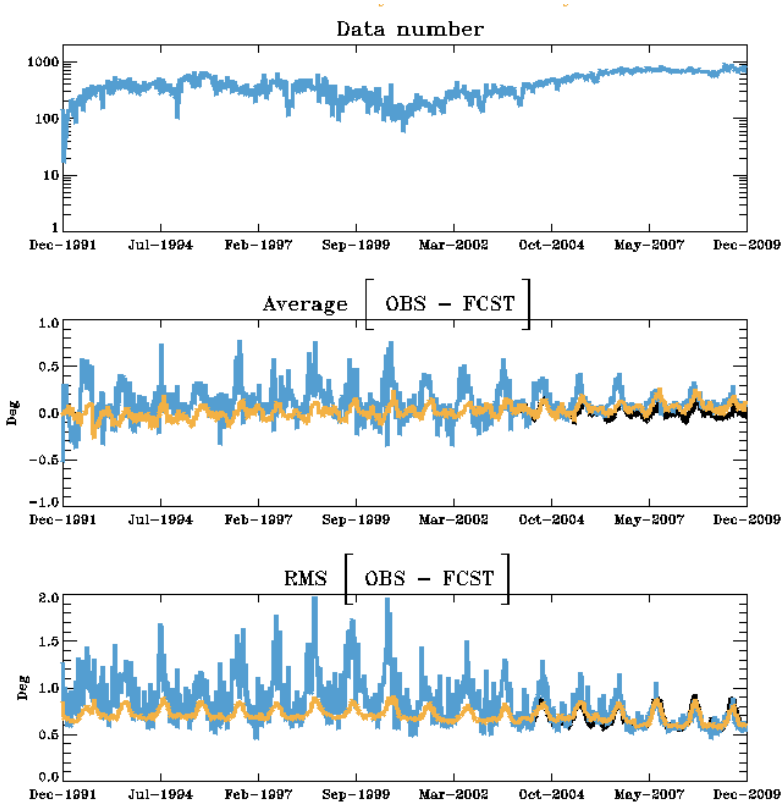

Figure 3: Data assimilation diagnostics for SLA for the global ocean from December 1992 until December 2009. Top: number of surface in situ data per assimilation cycle. Middle: mean innovation. Bottom: innovation RMS. NOAA Reynolds 0.25° assimilated SST is in orange, assimilated in situ near surface temperature is in blue, unassimilated NCEP RTG0.5° SST is in black.

Argo network sets up, the RMS decreases and the mean innovations become close to zero in each layer. We can clearly state that Argo network improves the reanalysis skill for the temperature field.

- [0-100m]: this layer exhibits the largest innovation RMS with a clear seasonal cycle. The mean innovation is slightly biased (~ 0.05°C) and this may be partly attributed to errors in the surface atmospheric surface parameters and the bulk formulation used.
- [100-300m]: innovation RMS is slightly weaker than in the [0-100m] layer. The mean bias is close to zero during the whole reanalysis except between 1997 and 1999 where it reaches -0.5~-0.1°C. This may be related to the strong 1997/1998 ENSO event whose large amplitude is difficult to be well reproduced.
- [300-800m]: Mean innovation is close to zero all along the reanalysis. Innovation RMS is stable before Argo era (0.6~0.7°C RMS) and then falls below 0.5 °C RMS.
- [800-2000m]: Mean innovation is slightly positive (~ 0.04°C) before Argo era and then becomes close to zero. Innovation RMS is stable before Argo era (~0.3°C RMS) and then falls below 0.2 °C RMS.

In summary, the temperature innovation statistics for the global ocean reveals that GLORYS2V1 reanalysis is stable (no drift). One identifies an improvement in the reanalysis skill (innovation mean and RMS) when Argo network sets up.

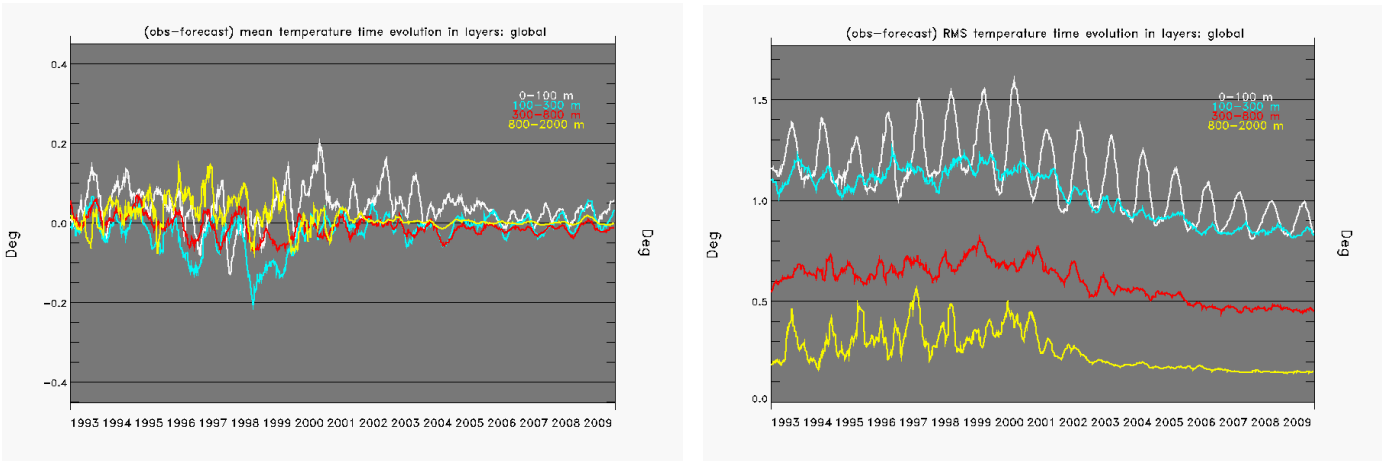

Figure 4: Global ocean innovation statistics for temperature. Globally averaged mean (a) and (b) RMS temperature innovation in [0-100m], [100-300m], [300-800m], [800-2000m] layers. Unit is degree Celsius.

As the data assimilation diagnostics are satisfying and reveal that GLORYS2V1 performs quite well, one expects its mean state to be weakly biased with respect to known climatologies. Figure 5 exhibits GLORYS2V1 and MJM95 (reference simulation) climatology (17-year mean) difference with Levitus et al. (2009) climatology for both temperature and salinity. This diagnostic helps identifying large scale biases and water masses property changes from the initial condition. Biases are much reduced in GLORYS2V1 than in MJM95 reference simulation, showing that data assimilation successfully constrains the mean state of the ocean. In GLORYS2V1, the bias is of the order of 0.4°C for temperature and less than ~0.05 PSU for salinity in most regions. For temperature, biases persist in some specific areas like the regions of large meso scale variability (Gulf Stream, Kuroshio, Antarctic circumpolar regions) but are much weaker than in the reference simulation with no data assimilation. Regarding the salinity, the behaviour is similar with a large decrease of the bias over the whole domain except locally like in the Gulf of Guinea, Mediterranean Sea, Caribbean, Gulf Stream and Indonesian through flow regions where the reference run exhibits reduced biases.

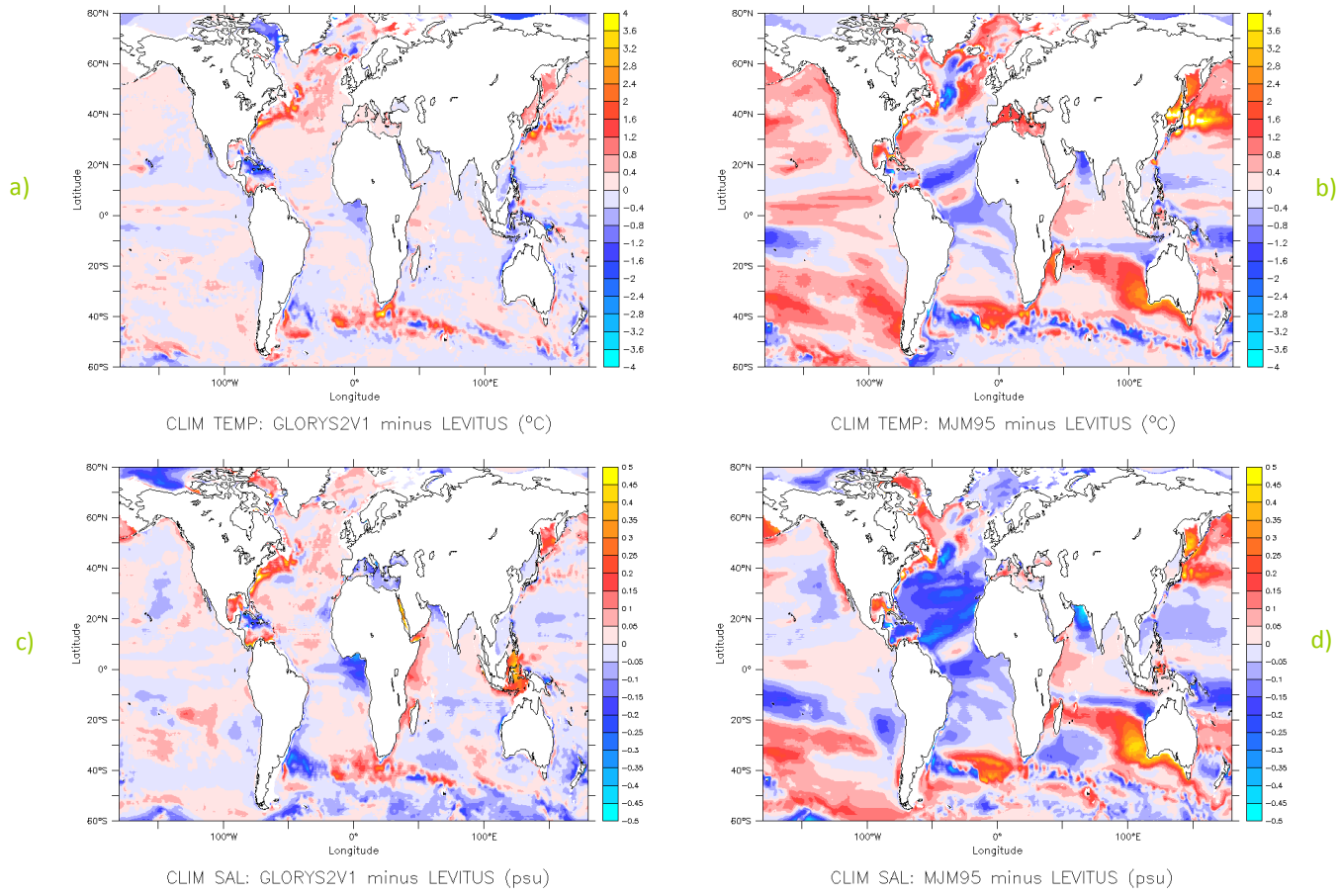

Figure 5: (a): GLORYS2V1 17-year mean temperature difference with Levitus 2009 climatology (°C), at 300m depth. (b): same as (a) but for the reference simulation MJM95. (c): GLORYS2V1 17-year mean salinity difference with Levitus 2009 climatology (PSU), at 300m depth. (d): same as (c) but for the reference simulation MJM95.

Volume transport through sections

The volume transport through seven WOCE sections for GLORYS2V1, MJM95 and the estimates provided by Lumpkin and Speer (2007) and Ganachaud and Wunsch (2000) are presented in Table 3 and Figure 6. There is a good agreement between the estimates based on inversion of hydrographic data and the ones provided by the OGCM simulations, with (GLORYS2V1) or without data assimilation (MJM95). The differences between the different estimates are generally explained by the associated uncertainties, showing that both simulations are able to well reproduce the global mean large scale circulation. We can however note that in the Antarctic circumpolar current (ACC) region (sections A21, E16 and Sr3) GLORYS2V1 transport estimate is systematically higher than the other estimates. This corresponds to an intensification of the ACC due to data assimilation. The origin of this mean transport increase is under investigation.

	Drake Passage (A21)	Atlantic 11° S (A8)	Indian 32° S (I5)	Pacific 24° N (P3)	Pacific 32° S (P6)	South A. - Antarctica 30° E (I6)	Tasmania Antarctica 143° E (Sr3)
GLORYS2V1	155 ± 6.	-1.4 ± 0.6	-15 ± 4	-0.2 ± 0.8	16 ± 3.5	157 ± 6	171 ± 6
MJM95	140 ± 6	-1.4 ± 0.5	-19 ± 3	-0.4 ± 0.6	21 ± 3	141 ± 6	161 ± 6
Lumpkin and Speer, 2007	129 ± 6	-0.5 ± 2.5	-13 ± 2.6	0.2 ± 2.6	14 ± 3	131 ± 8	141 ± 11
Ganachaud and Wunsh, 2000	140 ± 6	-	-16 ± 8.77	1 ± 5.1	17 ± 6	-	157 ± 10

Table 3: Mean volume transport across the seven WOCE sections in GLORYS2V1, MJM95 (17-year mean) and estimates provided by Lumpkin and Speer (2007) and Ganachaud and Wunsch (2000).

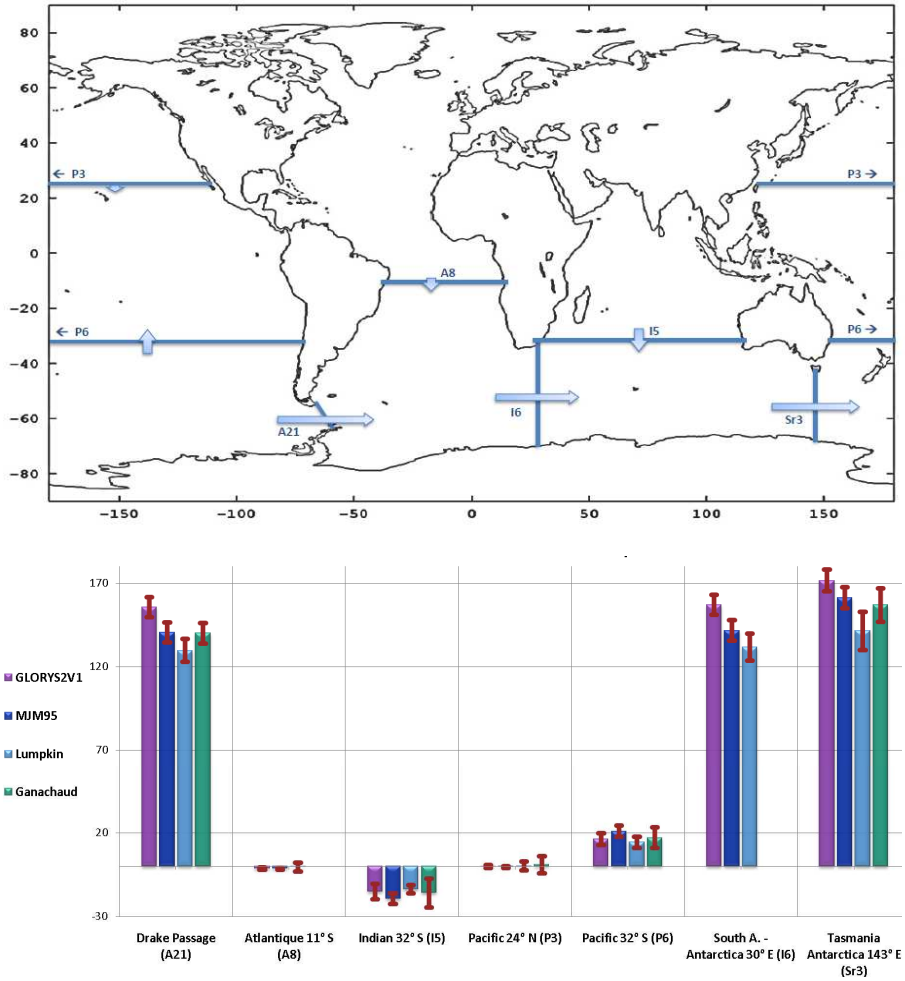

Figure 6: Volume transport through WOCE sections. (a) geographical location of the seven WOCE section. (b) Mean volume transport across the seven WOCE sections in GLORYS2V1, MJM95 (17-year mean) and estimates provided by Lumpin and Speer (2007) and Ganachaud and Wunsch (2000).

The meridional overturning circulation (MOC) in the North Atlantic is an important feature of the climate system as it transports surface warm water to the North and deep cold water to the South. Very few direct observations of this quantity are available (Bryden et al., 200) and their uncertainties are quite large. Since 2004, the RAPID-MOCHA array (Cunningham et al. 2007) deployment permits to monitor the daily to interannual variability of the Atlantic MOC at 26.5°N. The comparison with RAPID estimate (Fig. 7) is interesting as it shows the ability of GLORYS2V1 to simulate the AMOC. Between 2004 and 2009, the time evolution of the AMOC is quite well reproduced both in GLORYS2V1 and MJM95. Data assimilation increases the AMOC mean value and seasonal cycle amplitude, at least during RAPID time period. This leads to a reduction of the RMS difference with RAPID in the simulation with data assimilation (RMS difference is 3.6Sv) compared to MJM95 (RMS difference is 5.0Sv). However, this improvement of the MOC mean and seasonal variability has a drawback which is the reduction of the correlation with RAPID. The correlation between the AMOC estimate and GLORYS2V1 is 0.56 whereas it is higher for MJM95 (0.76). Other estimates of the AMOC provided by other global ocean reanalyses carried out in the framework of MyOcean project seem to suffer from the same shortcomings. This means that data assimilation, although reducing the model error would break some physical balances. This issue is currently being investigated using MyOcean global ocean eddy permitting reanalysis ensemble.

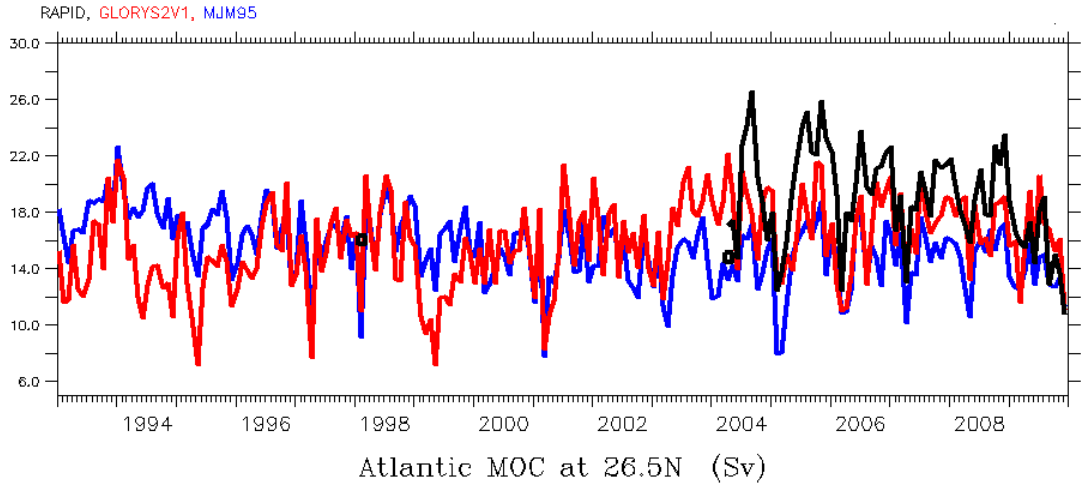

Figure 7: Maximum of the Atlantic MOC at 26.5°N (in Sverdrup) in GLORYS2V1 (red), MJM95 (blue) and RAPID data (black). Black squares in 1998 and 2004 represents the estimates of the AMOC based on hydrographic sections (Bryden et al., 2005).

Sea Ice

The LIM2-EVP module jointly with improved ice/ocean dynamical coupling and correction of surface air temperature and surface air humidity following the results from Lupkes et al. (2010) allows to realistically represent the Arctic sea ice extent interannual variability over the last 20 years (see Figure 8a). With strong interannual correlation (> 0.9) with observations, GLORYS2V1 slightly underestimates the stronger events like in September 1996 or in September 2007, this in turn reduces the trend slope (-49333 km^2/yr) compared to the satellite ones (Fig. 8a) and Comiso et al. (2008).

Despite the intrinsic larger variability in the Southern Ocean, the Antarctica sea ice extent interannual variability is also well reproduced over the 1993-2009 period with linear correlation with observations greater than 0.6 (Fig. 8b) and especially during the 2000's years. However, a large underestimation of sea ice cover during the first two years (1992-1993) makes the modeled Antarctica sea ice extent trend overestimated (59224 km^2/yr) compared to the weak positive satellite one (Fig. 8b). This may raise the question of establishing suitable initial conditions for sea ice and, more generally, for the Southern Ocean. No attempt was made to study the impact of increasing erroneously by 10% the downward LW flux southward 65°S.

In order to avoid numerical instabilities as in the previous configuration, the ice/ocean dynamical exchanges were limited. Instead of being damped, this coupling, now spatially smoothed at 1st order, allows a full exchange of momentum flux between ice and ocean. Together with the ability of the intrinsic EVP formulation to give a very quick response to the surface wind changes (3H), the consequences are a general acceleration of the sea ice speed compared to GLORYS1V1 and an overestimation compared to the satellite data (see Fig. 9) estimated at 60km horizontal resolution. These changes contribute however to a very high correlation (> 0.9) of GLORYS2V1 interannual variability with the observations (Fig. 9). This means that the reanalysis represents realistically the positive trend present in the satellite data. This is also consistent with the increasing trend mentioned by Rampal et al. (2009) with ice speed estimated from drifting buoys.

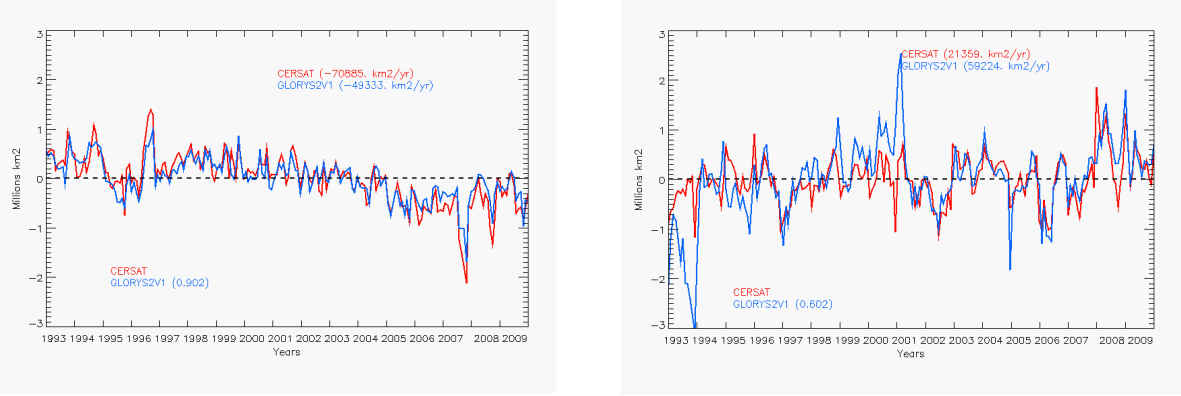

Figure 8: Sea ice extent monthly anomalies over the 1993-2009 periods from IFREMER/CERSAT dataset (red) and simulated by GLORYS2V1experiment (blue) for a) Arctic and b) Antarctica. Units are in Millions of km^2. Number in bracket in lower left panel indicates the linear correlation coefficient with the CERSAT dataset. Numbers in brackets in upper right indicate the linear trend over the period.

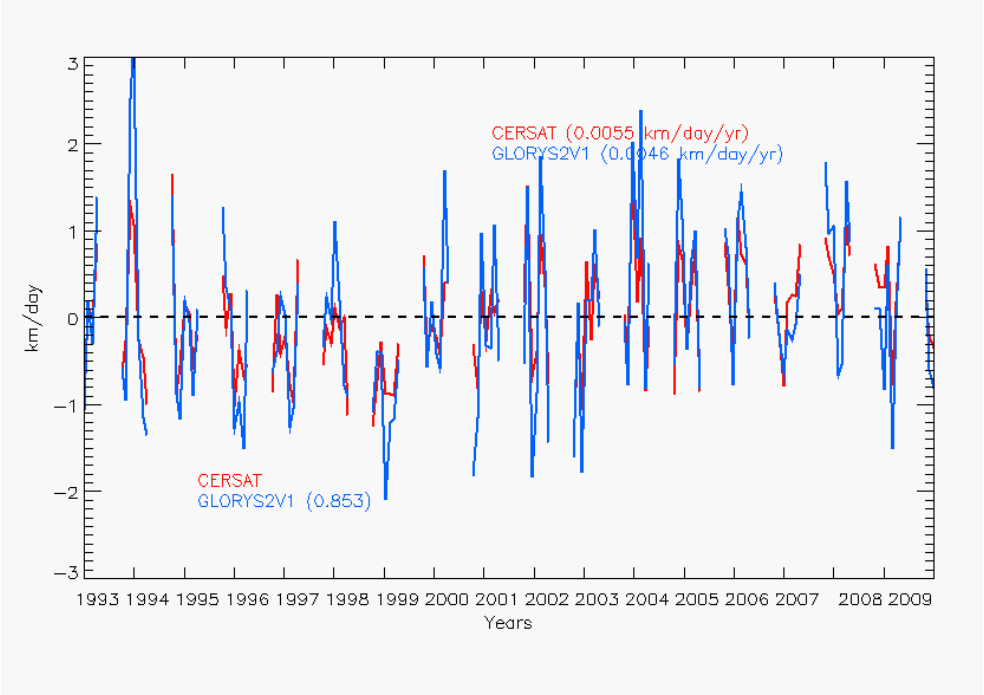

Figure 9: Arctic sea ice speed monthly anomalies over the 1993-2009 periods from IFREMER/CERSAT dataset (red) and simulated and by GLORYS2V1 (blue). Units are in km/day. The domain for GLORYS2V1 calculation is collocated with the CERSAT domain. Numbers indicate the linear trend over the period in km/day/year for each dataset. Number in bracket indicate the linear correlation coefficient with the CERSAT dataset.

Summary and conclusions

The results of GLORYS2V1 eddy permitting global ocean reanalysis over the altimetric era (1992-2009) are presented in this study. GLORYS2V1 reanalysis benefits from several improvements with respect to the former GLORYS1V1 reanalysis. The ocean model configuration ORCA025 has an increased vertical resolution of 75 vertical levels and is forced with ERA-Interim atmospheric parameters. The surface forcing includes specific corrections in order to remove large scale biases from shortwave and long wave radiative fluxes. The data assimilation scheme includes now a 3D-Var bias correction scheme which corrects the model state for large scale slowly varying biases in temperature and salinity. Last, new delayed time observations data sets are assimilated.

The validation results suggest that GLORYS2V1 reanalysis has a good skill in estimating and reproducing the observed variability of the main oceanic variables. The system is poorly biased for the temperature and salinity fields and innovation statistics suggest that the reanalysis is stable during the whole period. It appears that Argo network helps improving the ocean state estimation, i.e. the reanalysis skill is sensitive to the in situ observation network. In GLORYS2V1, the sea level (forecast) error is less than 7cm RMS on average. Interannual variability is well simulated; the global mean sea level rise is well reproduced. Although no ice data is assimilated, GLORYS2V1 sea ice properties (concentration and velocity) are very close to the available observations, suggesting that the reanalysis captures most of the monthly to interannual time scales.

The validation and assessment of GLORYS2V1 will be continued in the framework of the recently started MyOcean2 project. Comparisons with other global reanalyses will be performed in order to evaluate more accurately what are the strengths and weaknesses of eddy permitting global ocean reanalyses.

The challenges of GLORYS project are to continue to improve the reanalysis quality and to extend back in time the reanalyzed period. First objective will be achieved through the improvement of atmospheric surface forcing, the improvement of the data assimilation scheme (observation errors, forecast error covariance) and the assimilation of sea ice data. It is also planed to produce a 1979-present GLORYS reanalysis.

Acknowledgements

The authors acknowledge support from Météo France, CNRS, Mercator Ocean, CORIOLIS and CLS. Computations were performed with the support of Météo-France HPC Centre. The research leading to these results has received funding from the European Community's Seventh Framework Programme FP7/2007-2013 under grant agreement n°218812 (MyOcean), from Groupe Mission Mercator Coriolis, from Mercator-Ocean, and from INSU-CNRS.

The Florida Current cable and section data are made freely available on the Atlantic Oceanographic and Meteorological Laboratory (www.aoml.noaa.gov/phod/floridacurrent/) and are funded by the NOAA Office of Climate Observations. Data from the RAPID-WATCH MOC monitoring project are funded by the Natural Environment Research Council and are freely available from www.noc.soton.ac.uk/rapidmoc.

References

Arakawa A. and Lamb V. R., A potential enstrophy and energy conserving scheme for the shallow water equations, 1981, Month. Weath. Rev., 109, p.18-36.

Barnier B., Madec G. , Penduff T., Molines J.-M. and 15 co-autors of the DRAKKAR Group, 2006: Impact of partial steps and momentum advection schemes in a global ocean circulation model at eddy permitting resolution, Ocean dynamics, doi:10.1007/s10236-006-0082-1.

Benkiran M. and Greiner E., 2008: Impact of the Incremental Analysis Updates on a Real-Time System of the North Atlantic Ocean. Journal of Atmospheric and Oceanic Technology 25(11): 2055.

Bernie D. J., S. J. Woolnough, J. M. Slingo and E. Guilyardi, 2005: Modeling diurnal and intraseasonal variability of the ocean mixed layer, J. of Climate, 18, 1190-1202.

Bloom, S.C., Takas, L.L., Da Silva, A.M., Ledvina, D. 1996: Data assimilation using incremental analysis updates. Monthly Weather Review, 124, 1256–1271.

Bryden, H. L., H. R. Longworth, and S. A. Cunningham, 2005: Slowing of the Atlantic meridional overturning circulation at 25°N, Nature, 438, 655–657.

Chelton, D. B., M. G. Schlax, M. H. Freilich and R. F. Milliff, 2004: Satellite Measurements Reveal Persistent Small-Scale Features in Ocean Winds. *Science*, 303 :978-983 DOI: 10.1126/science.1091901

Comiso J. C., Parkinson C. L., Gersten R. and Stock L., 2008, Accelerated decline in the Arctic sea ice cover, Geoph. Res. Let., vol. 35(L01703), doi:10.1029/2007GL031972.

Cunningham S.A., Kanzow T., Rayner D., Baringer M.O., Johns W.E., Marotzke J., Longworth H.R. Grant E.M., Hirschi J.J.-M., Beal L.M., Meinen C.S., Bryden H.L, 2007: Temporal variability of the Atlantic Meridional Overturning Circulation at 26°N, Science, 317 , 935-938, doi:10.1126/science.1141304

Dai A. and Trenberth K. E., Estimates of freshwater discharge from continents: latitudinal and seasonal variations, 2002, J. Hydrometeorol., 3 (6), p. 660-687.

Dee D. P., Uppala S. M., Simmons A. J., Berrisford P. and 32 co-autors, 2011, The ERA-Interim reanalysis: configuration and performance of the data assimilation system, Quart. J. of Royal Met. Soc., 137, doi: 10.1002/qj.828, p. 553-597.

The DRAKKAR Group, 2007: B. Barnier and L. Brodeau and J. Le-Sommer and J.-M. Molines and T. Penduff and S. Theeten and A.-M. Treguier and G. Madec and A. Biastoch and C. Boning and L. Dengg and S. Gulev and R. Bourdalle-Badie and G. Garric and J. Chanut and S. Alderson and A. Coward and B. de Cuevas and A. New and K. Haines and G. Smith and S. Drijfhout and W. Hazeleger and C. Severijns and P. Myers, Eddy-permitting ocean circulation hindcasts of past decades, Clivar Exchanges Newsletter, 12(3), 8-10.

Ferry N., L. Parent, G. Garric, B. Barnier, N. C. Jourdain and the Mercator Ocean team, 2010: Mercator global eddy permitting ocean reanalysis GLORYS1V1: Description and results. Mercator Quarterly Newsletter 36, January 2010. http://www.mercator-ocean.fr/documents/lettre/lettre_36_en.pdf

Fichefet T. and Morales Maqueda M. A., 1997, Sensitivity of a global sea ice model to the treatment of ice thermodynamics and dynamics, J. Geophys. Res., 102-C6, p. 12,609-12,646.

Ganachaud, A., and C. Wunsch, 2000: Improved estimates of global ocean circulation, heat transport and mixing from hydrographic data. Nature, 408, 453–457.

Garric G., Verbrugge N. and C. Bricaud, 2011, Large scale ERAinterim radiative and precipitation surface fluxes assessment, correction and application on ¼° global ocean 1989-2009 hindcasts, EGU General Assembly, April 2011.

Gouretski, V.V., Koltermann, K.P., 2004. WOCE – Global Hydrographic Climatology. Berichte des Bundesamtes für Seeschifffahrt und Hydrographie, Technical Report 35/2004, 50 pp.

Jacobs, S.S., H.H. Hellmer, C.S.M. Doake, A. Jenkins, and R. Frolich, 1992: Melting of ice shelves and the mass balance of Antarctica. Journal of Glaciology, 38, 375-387

Hunke, E.C., and J.K. Dukowicz, (1997), An elastic-viscous-plastic model for sea ice dynamics, *J. Phys. Oceanogr.*, *27*, 1849-1867.

Koch-Larrouy A. and Madec G. and Blanke B. andMolcard R., Water mass transformation along the Indonesian throughflow in an OGCM, 2008, Ocean Dynamics, 58(3-4), p. 289-309.

Large W. G. and S. G. Yeager, 2004: Diurnal to decadal global forcing for ocean and sea ice models, , NCAR Technical note, 22p.

Levitus, S., J. I. Antonov, T. P. Boyer, R. A. Locarnini, H. E. Garcia, and A. V. Mishonov (2009), Global ocean heat content 1955–2008 in light of recently revealed instrumentation problems , Geophys. Res. Lett. , 36 , L07608, doi:10.1029/2008GL037155.

Levitus S., Boyer T. P.,Conkright M. E., O'Brian T., Antonov J. I., Stephens C., Stathopolos L. Johnson D. and Gelfeld R., World Ocean Database 1998 - NOAA Atlas NESDID18, National Oceanographic Data Center, Silver Spring, MD.

Lumpkin, R. and K. Speer, 2007: Global Ocean Meridional Overturning. J. Phy. Oceanog., vol. 37. 2550-2562.

Lupkes C., Vihma T., Jakobson E., König-Langlo G. and A. Tetzlaff, 2010, Meteorological observations from ship cruises during summer to the central Arctic: A comparison with reanalysis data, Geoph. Res. Lett., vol. 37(L09810), doi:10.1029/2010GL042724.

Madec G. and Imbard M., 1996, A global ocean mesh to overcome the North Pole singularity, Clim. Dyn., 12, p. 381-388.

Madec G. 2008. NEMO ocean engine. Note du Pole de modélisation, Institut Pierre-Simon Laplace (IPSL), France, No 27. pp205. ISSN No 1288 -1619.

Maloney, E. D., D. B. Chelton. (2006) An Assessment of the Sea Surface Temperature Influence on Surface Wind Stress in Numerical Weather Prediction and Climate Models. *Journal of Climate* **19**:12, 2743-2762

Oke, P.R., Brassington, G.B., Griffin, D.A. and Schiller, A. 2008: The Bluelink Ocean Data Assimilation System (BODAS), Ocean Modelling, 21, 46-70, doi:10.1016/j.ocemod.2007. 11.002.

Pham D. T., J. Verron, M. C. Roubaud, 1998: A singular evolutive extended Kalman filter for data assimilation in oceanography Journal of Marine Systems, 16, 323-340.

Rampal P., Weiss J. and Marsan D., 2009, Positive trend in the mean speed and deformation rate of Arctic sea ice, 1979-2007, J. Geophys. Res., 114-C05013, doi:10.1029/2008JC005066.

Reynolds, R. W., T. M. Smith, C. Liu, D. B. Chelton, K. S. Casey and M. G. Schlax, 2007: Daily High-resolution Blended Analyses for sea surface temperature. J. Climate, 20, 5473-5496.

Rio, M.-H., and F. Hernandez (2004), A mean dynamic topography computed over the world ocean from altimetry, in situ measurements, and a geoid model, J. Geophys. Res., 109, C12032, doi:10.1029/2003JC002226.

Rio, M. H., S. Guinehut, and G. Larnicol (2011), New CNES-CLS09 global mean dynamic topography computed from the combination of GRACE data, altimetry, and in situ measurements, J. Geophys. Res., 116, C07018, doi:10.1029/2010JC006505.

Roullet G. and G. Madec G., Salt conservation, free surface and varying volume: a new formulation for ocean GCMs, 2000, J. Geophys. Res., 105, p. 23,927-23,942.

Smith, Richard D., Mathew E. Maltrud, Frank O. Bryan, Matthew W. Hecht, 2000: Numerical Simulation of the North Atlantic Ocean at 1/10°. *J. Phys. Oceanogr.*, **30**, 1532–1561.

doi: http://dx.doi.org/10.1175/1520-0485(2000)030

Smith W. H. F. and Sandwell D. T., Global sea-floor topography from satellite altimetry and ship depth soundings, 1997, Science, 277, p.1956-1962.

Souza, J. M. A. C., C. de Boyer Montégut, C. Cabanes, and P. Klein, 2011: Estimation of the Agulhas ring impacts on meridional heat fluxes and transport using ARGO floats and satellite data, *Geophys. Res. Lett.*, 38, L21602, doi:10.1029/2011GL049359.

Talagrand, O. (1998): A posteriori evaluation and verification of analysis and assimilation algorithms. p. 17–28. In Proc. of ECMWF Workshop on Diagnosis of Data Assimilation System, Reading.

Testut, C-E., P. Brasseur, J-M Brankart and J. Verron , 2003 : Assimilation of sea-surface temperature and altimetric observations during 1992 –1993 into an eddy permitting primitive equation model of the North Atlantic Ocean. J. Mar. Sys., 40-41:291-316.

Vonder Haar, T. H., and A. H. Oort, 1973: New estimate of annual poleward energy transport by the northern hemisphere ocean. J. Phys. Oceanogr., 3, 169-172,.

NOTEBOOK

Articles

Meteo-France and Mercator Ocean contribution to the search of the AF447 wreckage

By M. Drévillon, E. Greiner, D. Paradis, C. Payan, J-M. Lellouche, G. Reffray, E. Durand, S. Law-Chune, S. Cailleau

Mercator Ocean operational global ocean system 1/12°PSY4V1: performances and applications in the context of the nuclear disaster of Fukushima

By C. Derval, C. Desportes, M. Drévillon, C. Estournel, C. Régnier, S. Law Chune

Drift forecast with Mercator Ocean velocity fields and addition of external wind/wave contribution

By S. Law Chune , Y. Drillet, P. De Mey and P. Daniel

GLORYS2V1 global ocean reanalysis of the altimetric era (1993-2009) at meso scale

By N. Ferry, L. Parent, G. Garric, C. Bricaud, C-E. Testut, O. Le Galloudec, J-M. Lellouche, M. Drévillon, E. Greiner, B. Barnier, J-M. Molines, N. Jourdain, S. Guinehut, C. Cabanes, L. Zawadzki.

Contact :

Please send us your comments to the following e-mail address: webmaster@mercator-ocean.fr

Next issue : April 2012